Characterisation of Diaminopimelate Aminotransferase from the novel bacterium *Verrucomicrobium Spinosum*

A thesis submitted in partial fulfilment of the requirements for the degree of

Master of Science in Biochemistry

in the School of Biological Sciences

Anthony William Weatherhead

University of Canterbury

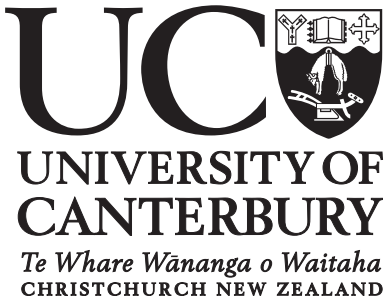

2018

“I guess hello world...”

-TW

Abstract

The intent of this research is to assess the enzyme diaminopimelate aminotransferase (DapL), an enzyme involved in the biosynthetic pathway of the essential amino acid L-lysine. Enzymes involved in L-lysine biosynthesis represent a valuable model for the elucidation of potential therapeutic targets, as animals cannot synthesise L-lysine *de novo* and require it through the diet. Recently, it has been found that all bacteria in the genus Chlamydia, including *Chlamydia trachomatis* the causative agent in sexually transmitted infection chlamydia, use the DapL enzyme to syntheise L-lysine. The closest free living relative to *C. trachomatis, Verrucomicrobium spinosum* is not pathogenic and has the unique feature of exclusively using DapL to synthesise L-lysine. *V. spinosum* is therefore a model organism for assessing the viability of DapL enzymes as therapeutic targets.

In this work, DapL from *V. spinosum* (*Vs*DapL) was successfully expressed and purified before elucidating any kinetic, structural and biophysical properties of the enzyme. Analysis of the biophysical properties of *Vs*DapL indicates that the enzyme exists in a monomer-dimer equilibrium in solution, however is predominantly dimeric at higher concentrations. This feature has never been reported in DapL orthologues. Finally, the first reported crystal structure for *Vs*DapL using X-ray crystallography is presented and confirms the dimeric structure at higher concentrations found in the biophysical experiments. Comparison of the *Vs*DapL structure with previously characterised DapL orthologues show that it is a typical type I aminotransferase.

Acknowledgements

This project has been a significant amount of work and would not be possible without help from a wide range of people. First and foremost I want to thank my supervisors Ren Dobson and André Hudson for the opportunity to work in both of your respective labs. The chance to work both in the Dobson lab here at the University of Canterbury and the Hudson Lab at the Rochester Institute of Technology in New York was unbelievable and I greatly appreciated every moment of the experience. Thank you both for guiding my progression throughout this project.

I extend a further thanks to my colleagues and friends in both the Dobson and Hudson research lab groups for providing extensive help and support over these past two years, it would have been a struggle without everyone. Thank you to Dr. Logan Heyes, Dr. Rachel North, Dr. Jen Crowther, Dr. Penel Cross and future Dr's. Chris Horne, James Davies, Amanda Board, Jenna Gilkes, Serena Watkin, Michael Love, Hannah Mckerchar, David Coombes, Michael Currie and Ollie Sterritt. Thanks for contributing your time and valuable scientific experience, it's been a great pleasure getting to know you all and I definitely would not have been able to complete this thesis without your help.

To the lab crew in Rochester Adrianna Coll De Peña, Austin Bartl and Lily Adams thanks for making my time in Rochester enjoyable. Definitely enjoyed the banter we shared and I know you will all do well in your respective fields in the future.

To my undergrad crew Emily Watters, Louis Perriman, Olivia Ogilvie, Rachel Bennie and Rory Smith thanks for all the good times even though the grind was tough.
To my brothers and my Dad, I can't thank you enough for the support throughout my academic career.

Lastly, to all of my friends, I appreciate the good times and banter we've had over the last few years and reminding me that there's a lot more to life than science. Whether you know it or not I don't think I would have had the motivation to complete this work without your support. Corona's are on me.

Table of Contents

Abbreviations

ADP	adenosine diphosphate
ATP	adenosine triphosphate
AUC	analytical ultracentrifugation
CD	circular dichroism
cm	centimetre
c(*M*)	continuous mass distribution
c(*s*)	continuous sedimentation coefficient distribution
CMP	cytidine monophosphate
Da	dalton
DapL	diaminopimelate aminotransferase
D_{max}	maximum particle diameter
DNA	deoxyribonucleic acid
EDTA	ethylenediaminetetraacetic acid
f/f_0	frictional ratio
g	gram
His-tag	Histidine tag
IMAC	immobilised metal affinity chromatography
IPTG	isopropyl β-D-1-thiogalactopyranoside
k_{cat}	catalytic turnover number
kDa	kilodalton
K_i	inhibition constant
K_M	Michaelis-Menten constant
k_{off}	rate constant for dissociation
L	litre
LB	luria bertani
M	molar
mg	milligram
min	minute
mL	millilitre
mm	millimetre
mM	millimolar

mol	moles
nm	nanometre
OD_{600}	optical density at 600 nm
PLP	pyridoxal-5-phosphate
$P(r)$	real space distance distribution function
r	radius
R_{factor}	residual factor
R_{free}	free R_{factor}
R_g	radius of gyration
rmsd	root-mean-square deviation
rpm	revolutions per minute
S	sedimentation coefficient, Svedberg
s	second
$s_{20,w}$	standardised sedimentation coefficient relative to water
$[S]$	substrate concentration
SAXS	small angle x-ray scattering
SDS	sodium dodecyl sulfate
SDS-PAGE	sodium dodecyl sulfate polyacrylamide gel electrophoresis
SOC	catabolite repression super optimal broth
T_M	melting temperature
Tris	2-amino-2-hydroxymethyl-propane-1,3-diol
UV	ultraviolet
v/v	volume to volume
w/v	weight to volume
Å	angstrom
°	degree
°C	degree celcius
µg	microgram
µL	microlitre
µM	micromolar
%	percent
σ	sigma
θ	theta

Table of Figures

Table of Tables

Chapter One – Introduction

1.1 Introduction

This thesis describes the first biophysical and structural characterisation of the enzyme diaminopimelate aminotransferase (DapL) from the bacteria *Verrucomicrobium spinosum*. DapL is the most recently identified enzyme in the lysine biosynthetic pathway and catalyses one of four alternative routes towards the synthesis of lysine. Various experimental approaches were employed in order to characterise DapL including analytical ultracentrifugation (AUC), X-ray crystallography, small angle X-ray scattering (SAXS), circular dichroism (CD) and steady-state kinetics.

1.2 Background

In nature, only nine out of the twenty known proteinogenic amino acids are considered to be essential for animals. Essential amino acids are nutritionally necessary, meaning they cannot be synthesised by mammalian enzymes *de novo* and therefore have to be ingested through the diet [1]. The aspartatic-derived amino acids, L-isoleucine (Ile, I) L-lysine (Lys, K), L-methionine (Met, M) and L-threonine (Thr, T) comprise four of the nine essential amino acids.

The biosynthesis of one particular aspartatic-derived amino acid, L-lysine (Figure 1.1), has recently been of high interest due to its nutritional importance in the diet and also its potential to be a target of commercial herbicides [2].

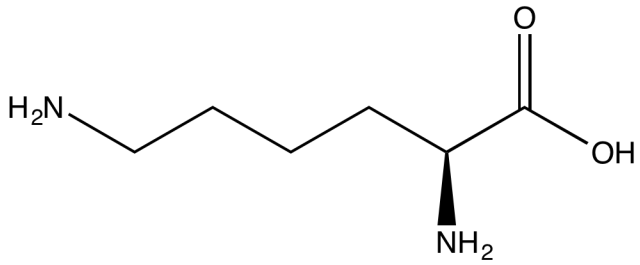

L-lysine

1.1: The chemical scaffold of L-lysine. L-lysine is comprised from six straight chain carbons with a terminal primary amine group (NH_2). The amine moiety enables contributes to its overall activity in several important physiological reactions. Constructed in CHEMDRAW.

The current understanding of the biosynthetic pathway of L-lysine stems from the identification of one of its precursor molecules *meso*-diaminopimelate (*meso*-Dap), in 1950 [3, 4]. Following the identification of *meso*-Dap, the development of narrow-spectrum antibiotics and herbicides that target enzymes within the L-lysine pathway has expanded, due to the low mammalian toxicity they possess [5, 6]. Narrow-spectrum antibiotics only target potential pathogens, while broad-spectrum antibiotics affect both potential pathogens and also the naturally occurring flora [7]. Availability of novel narrow-spectrum antibacterial agents that only affect a distinct group of bacterial species lowers the risks of disrupting the naturally occurring micro-biome, due to the potential detrimental effect on organisms involved in important physiological processes [8].

L-lysine and *meso*-Dap are possible targets of antibacterial agents, as most gram-negative and gram-positive bacteria require both to form a major structural component of the cell wall, peptidoglycan [9-12]. Peptidoglycan is a polymer that has an alternating disaccharide backbone of *N*-acetyl-glucosamine (NAG) and *N*-acetyl-muramic (NAM) acid, cross-linked by peptide chains [13]. Cross-linking of the backbone occurs via the amide functionality of L-lysine or *meso*-Dap and position four of a second side chain [14]. The importance of peptidoglycan in the structure of cell wall has presented a crucial target for the development of several therapeutic compounds including β-lactams and glycopeptides [11, 15]. As mammals cannot synthesize L-lysine, enzymes within the biosynthetic pathway represent a valuable model for the elucidation of novel therapeutic targets [16-19].

1.3 L-lysine biosynthetic pathways

1.3.1 Overview of L-lysine biosynthetic pathways

Two different pathways have evolved to synthesize L-lysine. L-lysine is either synthesised from 2-oxoglutarate and acetyl-CoA using the α-aminoadipate pathway (AAA), or from aspartate using the diaminopimelate (Dap) pathway. Fungi and euglena employ the AAA pathway, while archaea, bacteria and plants employ the diaminopimelate Dap pathway [20]. The two pathways are separated by a significant evolutionary gap suggesting that they developed separately in organisms that were unable to synthesize lysine [21].

1.3.2 The α-Aminoadipate (AAA) pathway

The existence of the AAA pathway for lysine biosynthesis has been established in several yeasts, fungi and euglena however the majority of the biochemical and genetic understanding of this pathway results from studies with the yeast *Saccharomyces cerevisiae* [22, 23]. The precursor molecule within the AAA pathway is 2-oxoglutarate, a key intermediate in the citric acid cycle. L-lysine is constructed of four carbons derived from 2-oxoglutarate and two carbons derived from acetate [21]. Despite the lack of knowledge surrounding the AAA pathway due to the pathway only being present in yeasts, euglena and higher fungi, two routes have been established (Figure 1.2) [24]. The action of two gene products is required in a few reactions that involve enzyme-bound intermediates [25].

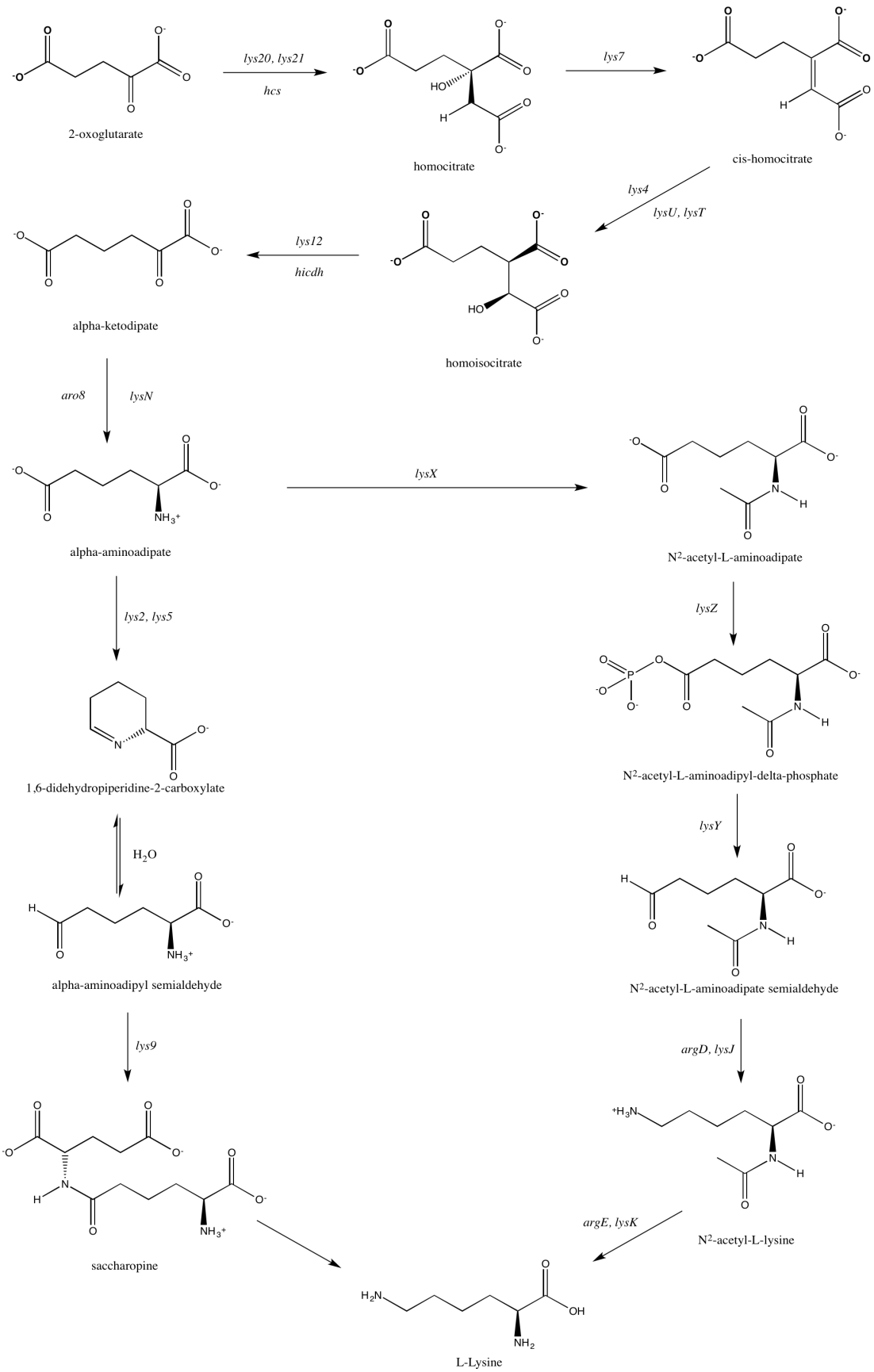

Figure 1.2: The AAA Pathway with all known substrates and enzymes. Figure taken from [26] and adapted in CHEMDRAW.

1.3.3 The diaminopimelate (Dap) pathway

The Dap pathway was first described in the bacteria *Escherichia coli* and is named after the characteristic intermediate, L,L-2, 6-diaminopimelic acid (L,L-Dap) [4, 12, 21, 27]. The carbon skeleton of L-lysine is constructed from carbons originating from L-aspartate and pyruvate as opposed to 2-oxoglutarate and acetate in the AAA pathway [12]. The enzymes and intermediates vary significantly from the AAA pathway, as the precursor molecule is L-aspartate, rather than 2-oxoglutarate. The three other aspartic-derived essential amino acids, Met, Thr and Ile are also formed through a branched segment of the Dap pathway and thus there have been several recent studies that have allowed for a better understanding [28].

The Dap pathway proceeds via up to nine enzymatic steps, each with a precursor substrate and specific enzyme (Figure 1.3). The pathway is divided into two sections, the upper section (reactions 1-4) that is common for all variants of the Dap pathway, and the lower section (reactions 5-9) that diverge into four sub-pathways [29].

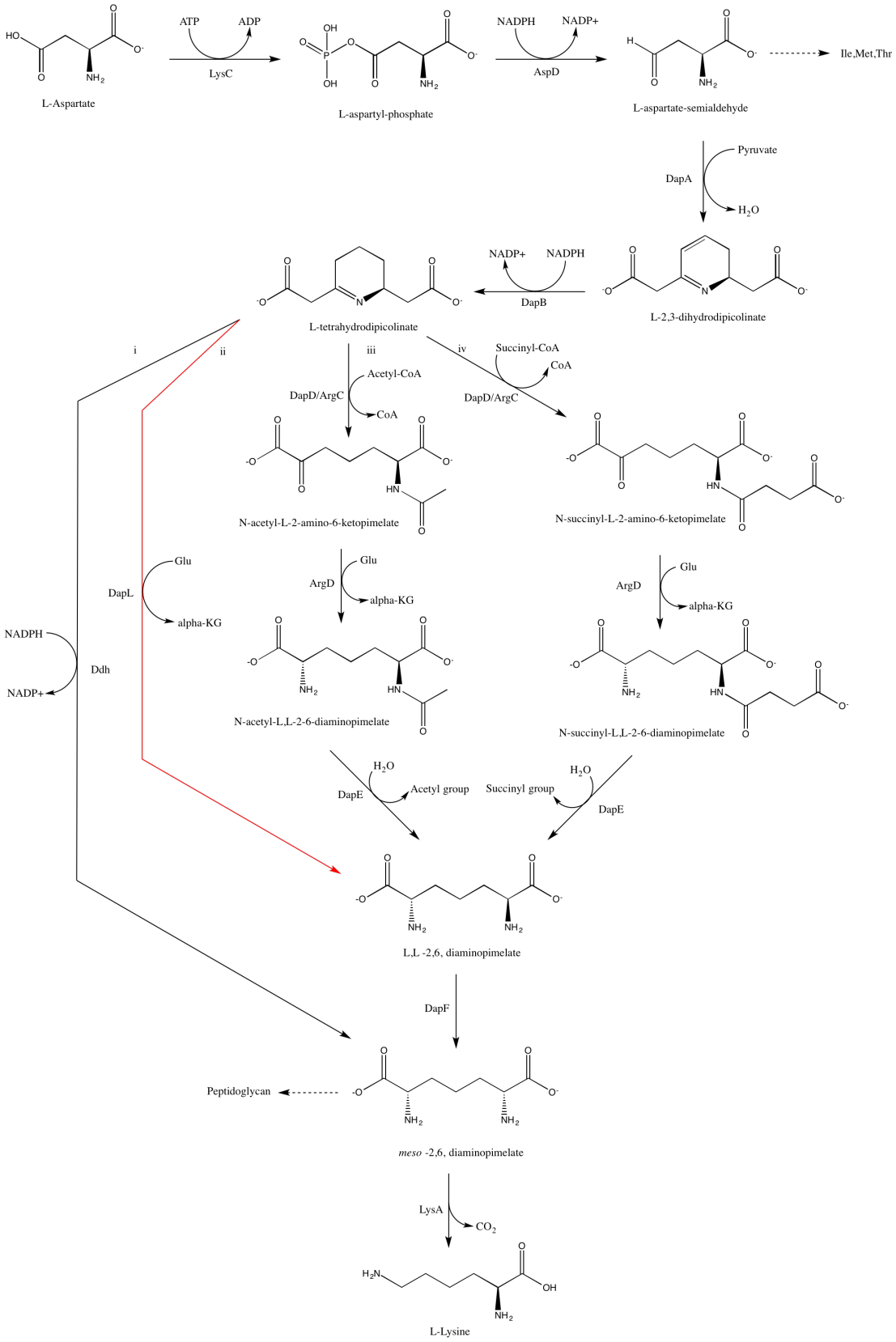

Figure 1.3: The Dap Pathway with all substrates enzymes. The four sub-pathways, the succinylase, acetylase, dehydrogenase and aminotransferase pathways of the L-lysine pathway are shown. The aminotransferase pathway is the focus of this thesis. Taken from [30] and adapted in CHEMDRAW.

1.3.4 The upper dap pathway

The first reaction in the Dap pathway is catalysed by the enzyme aspartate kinase (LysC, EC 2.7.2.4) and yields L-aspartyl-phosphate from L-aspartate with the input of metabolic energy in the form of ATP. The second reaction is catalysed by the enzyme aspartate semialdehyde dehydrogenase (AspD, EC 1.2.1.11) and takes the high-energy species L-aspartyl-phosphate and forms L-aspartate-semialdehyde [28]. These first two steps catalyse the synthesis of intermediate molecules that are common precursors for the formation of L-lysine, but also for the three other essential aspartic-derived amino acids, Thr, Met and Ile.

The key intermediate, L-tetrahydrodipicolinate (THDP), is formed via the third and fourth reactions in the pathway, and proceeds through the reaction of L-aspartate semialdehyde with pyruvate, followed by further reaction with the high-energy molecule NADPH. Dihydrodipicolinate synthase (DHDPS, EC 4.3.3.7) encoded by the DapA gene and dihydrodipicolinate reductase (DHDPR, EC 1.17.1.8) encoded by the DapB gene catalyse these two reactions. DHDPS catalyses the first committed step in the lysine biosynthetic pathway, where the substrates L-aspartate-semialdehyde and pyruvate are condensed to form an unstable heterocycle HTPA [31]. This highly unstable product is a substrate for DHDPR in a pyridine nucleotide-dependent reduction of dihydrodipicolinic acid (DHP) that generates the product THDP [32]. Recent characterisation has found that bacterial and plant DHDPR exists in two different oligomeric states, suggesting complexity in the pathway between species [33, 34]. The cyclic intermediate THDP generated by DHDPR in the fourth reaction, can be reversibly hydrolysed to its open chain form L-α-amino-ε-keto-pimelate in the presence of water (Figure 1.4).

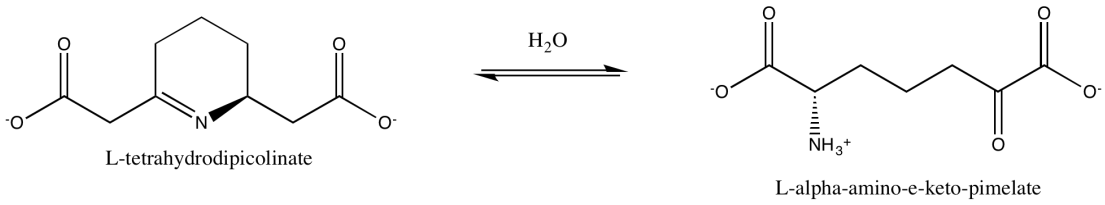

Figure 1.4: The reversible hydrolysis reaction of tetrahydrodipicolinate and L-α-amino-ε-keto-pimelate. The cyclic form (left) has the nitrogen moiety tied up in a 6 membered ring structure while the open acyclic form (right) has the nitrogen moiety exposed as a protonated amine (NH_3^+) at physiologic pH values. Both forms are recognised at further stages in the reaction.

1.3.5 The lower dap pathway

Following the formation of THDP, subsequent reactions of the Dap pathway can vary depending on the branch of the pathway taken, however, all branches form the intermediate *meso*-Dap due to it being the immediate precursor molecule for PG and therefore crucial for cell wall synthesis [35]. There have been four known sub-pathways from the intermediate THDP to form *meso*-Dap that have been described within archaea bacteria and plants (Figure 1.3) [36]. Two of these pathways, the succinylase and acetylase pathways, have been identified to be the major routes taken by gram positive and negative bacteria, where multiple N-succinylated or N-acetylated intermediates are formed [37].

However, two other pathways, the aminotransferase pathway catalysed by the enzyme diaminopimelate aminotransferase (DapL, EC 2.6.1.83) and the dehydrogenase pathway catalysed by the enzyme diaminopimelate dehydrogenase (DapDdh, EC 1.4.1.16), have been identified however are less frequently used [38]. It was previously believed that only one of the four pathways is active at a given time, however, recent research with the bacteria *Corynebacterium glutamicum* has suggested that pathways can be active at the same time to handle a potential increase in flow of metabolites entering the pathway [39, 40]. The succinylase and acetylase pathways are analogous to each other and require several steps using multiple enzymes to form L,L-Dap, while the aminotransferase route only requires one step [36]. Preferentially using the pathways that require multiple enzymes and steps, over the one-step pathway, demonstrates the intricacy behind the control and regulation of the lysine biosynthetic pathway.

The dehydrogenase pathway variation mediates a similar conversion however forms *meso*-Dap rather than L,L-Dap in one step [41]. If the dehydrogenase pathway is not active then *meso*-Dap is synthesised through isomerisation of L,L-Dap by the enzyme diaminopimelate epimerase (DapF, EC 5.1.1.7) [42]. In bacteria, *meso*-Dap is either incorporated into the PG or it is decarboxylated via the enzyme *meso*-diaminopimelate decarboxylase (LysA, EC 4.1.1.20) to the final product of the pathway L-lysine [30]. If the later is the case, *meso*-Dap is stereospecifically decarboxylated at the D centre with inversion of configuration.

1.3.6 The aminotransferase pathway

The aminotransferase pathway catalysed by DapL was only recently uncovered through extensive genomic analysis in the plant *Arabidopsis thaliana* in 2006 by Hudson et al. [30]. DapL catalyses the reversible transamination of THDP to L,L-Dap in one-step and therefore bypasses the use of multiple enzymes (Figure 1.5). The reaction proceeds through a bimolecular ping-pong mechanism and acts to transfer the amino group from the L-glutamate, which acts as an amino donor to the product L,L-Dap, which acts as an amino acceptor (Chapter 3).

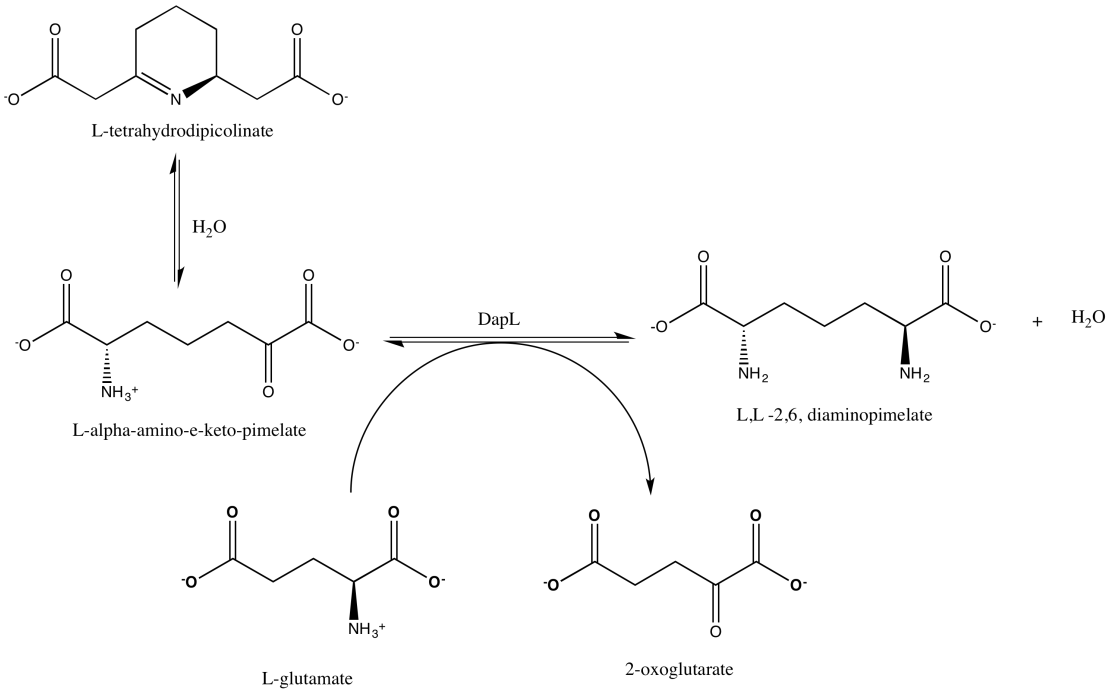

Figure 1.5: The reversible chemical reaction of THDP to L,L-Dap catalysed by DapL. L-glutamate acts as the amino donor in the reaction and is converted to α-ketoglutarate. The cofactor pyridoxal-5-phosphate (PLP) is used as an amino acceptor in the reaction**.**

Identification of DapL in plants prompted investigation within bacteria, and has since only been found in 13% of all bacterial genomes (calculated from genome annotation in the Integrated Microbial Genomes database) [8, 43]. Thus the majority of bacteria employ alternative variants of the Dap pathway to synthesise PG and L-lysine. Interestingly, the genera *Chlamydia,* the causative agent in the sexually transmitted infection chlamydia*, Leptospira,* the cause of the kidney disease leptospirosis*,* and *Treponema* the principal cause of the sexually transmitted infection syphilis, all use the aminotransferase pathway to synthesise L-lysine [8]. Thus any potential inhibitor of DapL could have vast potential as a narrow-spectrum antibiotic target in bacteria that use the pathway.

1.4 Crystal structures of DapL

Phylogenetic analysis of DapL enzymes indicated that two classes of DapL existed based on sequence similarity, type I and type II [43, 44]. Type I DapL is common among plants and chlamydia while type II are more common in bacteria [44]. Crystal structure studies of DapL enzymes have since been carried out in three organisms, *A. thaliana*,

Chlamydomonas reinhardtii and *Chlamydia trachomatis* (Figure 1.6). Comparison of the crystal structures has provided insight into structural differences that occur between orthologues and have aided in the search potential for therapeutic targets.

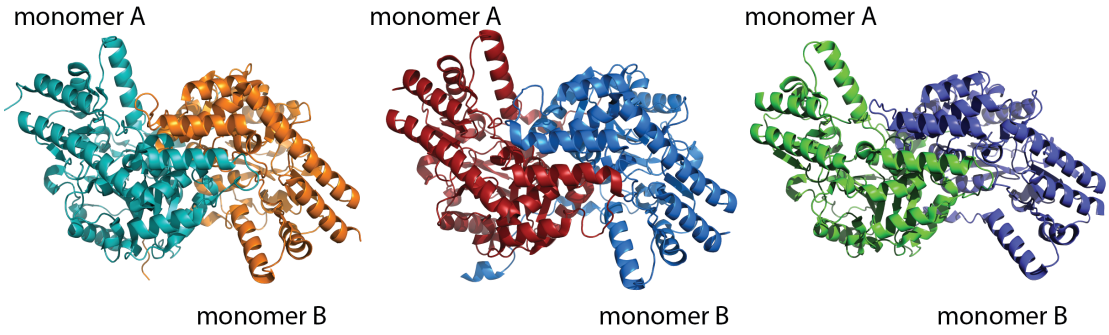

Figure 1.6: The dimeric crystal structure of DapL. Left to right: *A. thaliana*, *C. reinhardtii and C. trachomatis* DapL. The two monomers are labeled A and B and are separated based on colour. Images were generated using Pymol [45].

1.4.1 *Arabidopsis thaliana* DapL

After the initial discovery of the aminotransferase pathway in the plant *A. thaliana*, the structure of DapL was solved to 1.95 Å by Watanabe et al. 2007 and was used as a foundation for further work for other organisms that employ the aminotransferase pathway [46, 47]. It was found that DapL from *A. thaliana* (AtDapL) exists as a homodimer in both the apo- form and with a cofactor pyridoxal-5-phosphate (PLP), a feature shared by many aminotransferase enzymes (Figure 6). The enzyme contains two active sites, comprised from residues from both monomers indicating that a dimeric structure must be adopted to be active. The overall structure of the fold of *At*DapL closely resembles that of type I aminotransferases, indicating that structure is conserved within PLP dependent enzymes [46].

1.4.2 *Chlamydomonas reinhardtii* DapL

Stemming from the research with *At*DapL, the crystal structure of DapL from the unicellular alga *C. reinhardtii* (*Cr*DapL) was solved to 1.55 Å by Dobson et al. 2011, with the intention to aid in the potential development of algaecides. The overall

structure for *Cr*DapL in its apo- form displayed a similar homodimer characteristic of *A. thaliana* and was classified as a type I aminotransferase [48] .

1.4.3 *Chlamydia trachomatis* DapL

Recent research has identified that all bacteria in the genera *Chlamydia* employ the aminotransferase pathway in biosynthetic pathway of L-lysine to synthesise peptidoglycan [30]. The bacterium *C. trachomatis* is one of four species in the *Chlamydiae* genus and is most commonly associated with being the cause of the most frequently reported sexually transmitted infection (STI) known as chlamydia [49]. *C. trachomatis* has also been well documented in several severe human diseases including trachoma, the leading cause of preventable blindness [50].

The crystal structure of DapL from *C trachomatis* (*Ct*DapL) is the most recent DapL structure published and was solved to 2.05 Å by Watanabe et al. 2011, in both its apo-form and additionally with the co-factor PLP [51]. *Ct*DapL was found to adopt a homodimer oligomeric state in line with type I aminotransferases. However despite *C. trachomatis* DapL sharing over 40% sequence identity and with *At*DapL, substrate specificity differed significantly between the two organisms. *Ct*DapL displayed promiscuous substrate specificity in comparison to *At*DapL is suggested to be due to several flexible residues that comprise the pocket of the active sites that differ between organisms [44]. This feature of substrate specificity still remains unclear, however further structural studies in different organisms may provide some insight into this feature.

1.5 Research goals and perspective of this thesis

While mammals cannot synthesise L-lysine in *vivo* and acquire it through the diet, many organisms including bacteria, plants, and archaea can synthesise it via the AAA and Dap pathways outlined above. The work presented in this thesis focuses on the first structural and biophysical characterisation of DapL from the bacterium *Verrucomicrobium spinosum.*

V. spinosum is a free-living, non-pathogenic bacterium, closely related to *C. trachomatis,* however it bears the specific feature of only synthesising *meso*-Dap and L-lysine through the aminotransferase pathway using the enzyme DapL [30, 52-54]. *V. spinsosum* is not pathogenic and the feature of solely employing the aminotransferase pathway for L-lysine biosynthesis allows it to be used as a model organism in which DapL enzymes from pathogenic organisms can studied in. This may aid the development of antibacterial, herbicidal or algaecidal compounds [8].

The structural elucidation of *V. spinosum* DapL (*Vs*DapL) for therapeutic discovery was the principal focus of this thesis, however the work performed also aids in assessing whether DapL is a feasible target for compounds in all human pathogenic bacteria that use the aminotransferase pathway.

Chapter 2 of this thesis discusses the specific protocol and results for the successful expression and purification of DapL from *V. spinosum.*

Chapter 3 entails the kinetic assays and analysis of *Vs*DapL using steady-state initial rate kinetic experiments with and also without inhibitors.

Chapter 4 explores the biophysical properties of *Vs*DapL in solution using the techniques circular dichroism (CD), analytical ultracentrifugation (AUC) and small angle X-ray scattering (SAXS).

Chapter 5 describes in detail the first X-ray crystallography structure of *Vs*DapL and explores the intricate workings of the active site.

1.6 References

[1] Reeds, P. J. (2000) Dispensable and indispensable amino acids for humans, *J Nutr 130*, 1835S-1840S.

[2] Jander, G., and Joshi, V. (2010) Recent progress in deciphering the biosynthesis of aspartate-derived amino acids in plants, *Mol Plant 3*, 54-65.

[3] Work, E. (1950) A new naturally occurring amino acid, *Nature 165*, 74.

[4] Gilvarg, C. (1960) Biosynthesis of diaminopimelic acid, *Fed Proc 19*, 948-952.

[5] Viola, R. E. (2001) The central enzymes of the aspartate family of amino acid biosynthesis, *Acc Chem Res 34*, 339-349.

[6] Jander, G., and Joshi, V. (2009) Aspartate-derived amino acid biosynthesis in *Arabidopsis thaliana*, *The Arabidopsis Book*, e0121.

[7] Van Saene, R., Fairclough, S., and Petros, A. (1998) Broad- and narrow-spectrum antibiotics: a different approach, *Clin Microbiol Infect 4*, 56-57.

[8] Triassi, A. J., Wheatley, M. S., Savka, M. A., Gan, H. M., Dobson, R. C., and Hudson, A. O. (2014) L,L-diaminopimelate aminotransferase (DapL): a putative target for the development of narrow-spectrum antibacterial compounds, *Front Microbiol 5*, 509.

[9] Henrichfreise, B., Schiefer, A., Schneider, T., Nzukou, E., Poellinger, C., Hoffmann, T. J., Johnston, K. L., Moelleken, K., Wiedemann, I., Pfarr, K., Hoerauf, A., and Sahl, H. G. (2009) Functional conservation of the lipid II biosynthesis pathway in the cell wall-less bacteria Chlamydia and Wolbachia: why is lipid II needed?, *Mol Microbiol 73*, 913-923.

[10] Asong, J., Wolfert, M. A., Maiti, K. K., Miller, D., and Boons, G. J. (2009) Binding and Cellular Activation Studies Reveal That Toll-like Receptor 2 Can Differentially Recognize Peptidoglycan from Gram-positive and Gram-negative Bacteria, *J Biol Chem 284*, 8643-8653.

[11] Cox, R. J., Sutherland, A., and Vederas, J. C. (2000) Bacterial diaminopimelate metabolism as a target for antibiotic design, *Bioorg Med Chem 8*, 843-871.

[12] Hutton, C. A., Perugini, M. A., and Gerrard, J. A. (2007) Inhibition of lysine biosynthesis: an evolving antibiotic strategy, *Mol Biosyst 3*, 458-465.

[13] Humann, J., and Lenz, L. L. (2009) Bacterial peptidoglycan degrading enzymes and their impact on host muropeptide detection, *J Innate Immun 1*, 88-97.

[14] Kimura, K., and Bugg, T. D. (2003) Recent advances in antimicrobial nucleoside antibiotics targeting cell wall biosynthesis, *Nat Prod Rep 20*, 252-273.

[15] Pilhofer, M., Aistleitner, K., Biboy, J., Gray, J., Kuru, E., Hall, E., Brun, Y. V., VanNieuwenhze, M. S., Vollmer, W., Horn, M., and Jensen, G. J. (2013) Discovery of chlamydial peptidoglycan reveals bacteria with murein sacculi but without FtsZ, *Nat Commun 4*, 2856.

[16] Galili, G. (2002) New insights into the regulation and functional significance of lysine metabolism in plants, *Annu Rev Plant Biol 53*, 27-43.

[17] Yang, H., and Ludewig, U. (2014) Lysine catabolism, amino acid transport, and systemic acquired resistance: What is the link?, *Plant Signal Behav 9*.

[18] Galili, G. (1995) Regulation of Lysine and Threonine Synthesis, *Plant Cell 7*, 899-906.

[19] Nachar, V. R., Savka, F. C., McGroty, S. E., Donovan, K. A., North, R. A., Dobson, R. C., Buckley, L. J., and Hudson, A. O. (2012) Genomic and Biochemical Analysis of the Diaminopimelate and Lysine Biosynthesis Pathway in *Verrucomicrobium spinosum*: Identification and Partial Characterization of L,L-Diaminopimelate Aminotransferase and UDP-N-Acetylmuramoylalanyl-D-glutamyl-2,6-meso-Diaminopimelate Ligase, *Front Microbiol 3*, 183.

[20] Liu, Y., Xie, S., and Yu, J. (2016) Genome-Wide Analysis of the Lysine Biosynthesis Pathway Network during Maize Seed Development, *PloS one 11*, e0148287.

[21] Vogel, H. J. (1964) Distribution of Lysine Pathways Among Fungi: Evolutionary Implications, *The American Naturalist 98*, 435-446.

[22] Cox, R. J. (1996) The DAP pathway to lysine as a target for antimicrobial agents, *Natural product reports 13*, 29-43.

[23] Torruella, G., Suga, H., Riutort, M., Pereto, J., and Ruiz-Trillo, I. (2009) The evolutionary history of lysine biosynthesis pathways within eukaryotes, *J Mol Evol 69*, 240-248.

[24] Xu, H., Andi, B., Qian, J., West, A. H., and Cook, P. F. (2006) The alpha-aminoadipate pathway for lysine biosynthesis in fungi, *Cell Biochem Biophys 46*, 43-64.

[25] Zabriskie, T. M., and Jackson, M. D. (2000) Lysine biosynthesis and metabolism in fungi, *Nat Prod Rep 17*, 85-97.

[26] Dairi, T., Kuzuyama, T., Nishiyama, M., and Fujii, I. (2011) Convergent strategies in biosynthesis, *Nat Prod Rep 28*, 1054-1086.

[27] Vogel, H. J. (1959) On Biochemical Evolution: Lysine Formation in Higher Plants, *Proc Natl Acad Sci U S A 45*, 1717-1721.

[28] Sun, G., and Huang, J. (2011) Horizontally acquired DAP pathway as a unit of self-regulation, *J Evol Biol 24*, 587-595.

[29] Born, T. L., and Blanchard, J. S. (1999) Structure/function studies on enzymes in the diaminopimelate pathway of bacterial cell wall biosynthesis, *Curr Opin Chem Biol 3*, 607-613.

[30] McCoy, A. J., Adams, N. E., Hudson, A. O., Gilvarg, C., Leustek, T., and Maurelli, A. T. (2006) L,L-diaminopimelate aminotransferase, a trans-kingdom enzyme shared by Chlamydia and plants for synthesis of diaminopimelate/lysine, *Proc Natl Acad Sci U S A 103*, 17909-17914.

[31] Dobson, R. C., Griffin, M. D., Roberts, S. J., and Gerrard, J. A. (2004) Dihydrodipicolinate synthase (DHDPS) from *Escherichia coli* displays partial mixed inhibition with respect to its first substrate, pyruvate, *Biochimie 86*, 311-315.

[32] Reddy, S. G., Scapin, G., and Blanchard, J. S. (1996) Interaction of pyridine nucleotide substrates with *Escherichia coli* dihydrodipicolinate reductase: thermodynamic and structural analysis of binary complexes, *Biochemistry 35*, 13294-13302.

[33] Pavelka, M., Weisbrod, T. R., and Jacobs, W. (1997) Cloning of the dapB gene, encoding dihydrodipicolinate reductase, from Mycobacterium tuberculosis, *Journal of bacteriology 179*, 2777-2782.

[34] Watkin, S. A. J., Keown, J. R., Richards, E., Goldstone, D. C., Devenish, S. R. A., and Grant Pearce, F. (2018) Plant DHDPR forms a dimer with unique secondary structure features that preclude higher-order assembly, *Biochem J 475*, 137-150.

[35] Velasco, A., Leguina, J., and Lazcano, A. (2002) Molecular evolution of the lysine biosynthetic pathways, *Journal of Molecular Evolution 55*, 445-449.

[36] Liu, Y., White, R. H., and Whitman, W. B. (2010) Methanococci use the diaminopimelate aminotransferase (DapL) pathway for lysine biosynthesis, *Journal of bacteriology 192*, 3304-3310.

[37] Gillner, D. M., Becker, D. P., and Holz, R. C. (2013) Lysine biosynthesis in bacteria: a metallodesuccinylase as a potential antimicrobial target, *J Biol Inorg Chem 18*, 155-163.

[38] Scapin, G., Cirilli, M., Reddy, S. G., Gao, Y., Vederas, J. C., and Blanchard, J. S. (1998) Substrate and inhibitor binding sites in *Corynebacterium glutamicum* diaminopimelate dehydrogenase, *Biochemistry 37*, 3278-3285.

[39] Wehrmann, A., Phillipp, B., Sahm, H., and Eggeling, L. (1998) Different Modes of Diaminopimelate Synthesis and Their Role in Cell Wall Integrity: a Study with *Corynebacterium glutamicum*, *Journal of bacteriology 180*, 3159-3165.

[40] Schrumpf, B., Schwarzer, A., Kalinowski, J., Puhler, A., Eggeling, L., and Sahm, H. (1991) A functionally split pathway for lysine synthesis in *Corynebacterium glutamicium*, *J Bacteriol 173*, 4510-4516.

[41] Rodionov, D. A., Vitreschak, A. G., Mironov, A. A., and Gelfand, M. S. (2003) Regulation of lysine biosynthesis and transport genes in bacteria: yet another RNA riboswitch?, *Nucleic Acids Res 31*, 6748-6757.

[42] Richaud, C., Higgins, W., Mengin-Lecreulx, D., and Stragier, P. (1987) Molecular cloning, characterization, and chromosomal localization of dapF, the Escherichia coli gene for diaminopimelate epimerase, *J Bacteriol 169*, 1454-1459.

[43] Hudson, A. O., Gilvarg, C., and Leustek, T. (2008) Biochemical and phylogenetic characterization of a novel diaminopimelate biosynthesis pathway in prokaryotes identifies a diverged form of LL-diaminopimelate aminotransferase, *J Bacteriol 190*, 3256-3263.

[44] Dobson, R. C., Giron, I., and Hudson, A. O. (2011) L,L-diaminopimelate aminotransferase from *Chlamydomonas reinhardtii*: a target for algaecide development, *PLoS One 6*, e20439.

[45] L DeLano, W. (2002) *The PyMOL Molecular Graphics System (2002) DeLano Scientific, Palo Alto, CA, USA*. http://www.pymol.org.

[46] Watanabe, N., Cherney, M. M., van Belkum, M. J., Marcus, S. L., Flegel, M. D., Clay, M. D., Deyholos, M. K., Vederas, J. C., and James, M. N. (2007) Crystal structure of LL-diaminopimelate aminotransferase from *Arabidopsis thaliana*: a recently discovered enzyme in the biosynthesis of L-lysine by plants and Chlamydia, *J Mol Biol 371*, 685-702.

[47] Watanabe, N., Clay, M. D., van Belkum, M. J., Cherney, M. M., Vederas, J. C., and James, M. N. G. (2008) Mechanism of Substrate Recognition and PLP-induced Conformational Changes in LL-Diaminopimelate Aminotransferase from *Arabidopsis thaliana*, *Journal of Molecular Biology 384*, 1314-1329.

[48] Rochaix, J. D. (2001) Assembly,function, and dynamics of the photosynthetic machinery in *Chlamydomonas reinhardtii, Plant Physiol 127*, 1394-1398.

[49] Workowski, K. A., and Berman, S. M. (2007) Centers for Disease Control and Prevention sexually transmitted diseases treatment guidelines, *Clin Infect Dis 44 Suppl 3*, S73-76.

[50] Wagner, M., and Horn, M. (2006) The Planctomycetes, *Verrucomicrobia, Chlamydiae* and sister phyla comprise a superphylum with biotechnological and medical relevance, *Curr Opin Biotechnol 17*, 241-249.

[51] Watanabe, N., Clay, M. D., van Belkum, M. J., Fan, C., Vederas, J. C., and James, M. N. (2011) The structure of LL-diaminopimelate aminotransferase from *Chlamydia trachomatis*: implications for its broad substrate specificity, *J Mol Biol 411*, 649-660.

[52] Domman, D. B., Steven, B. T., and Ward, N. L. (2011) Random transposon mutagenesis of *Verrucomicrobium spinosum* DSM 4136(T), *Arch Microbiol 193*, 307-312.

[53] Yee, B., Lafi, F. F., Oakley, B., Staley, J. T., and Fuerst, J. A. (2007) A canonical FtsZ protein in V*errucomicrobium spinosum*, a member of the Bacterial phylum Verrucomicrobia that also includes tubulin-producing Prosthecobacter species, *BMC Evol Biol 7*, 37.

[54] Sait, M., Kamneva, O. K., Fay, D. S., Kirienko, N. V., Polek, J., Shirasu-Hiza, M. M., and Ward, N. L. (2011) Genomic and Experimental Evidence Suggests that *Verrucomicrobium spinosum* Interacts with Eukaryotes, *Front Microbiol 2*, 211.

Chapter Two – Expression and Purification of DapL from *Verrucomicrobium spinosum*

2.1 Introduction

Due to the potential benefits of targeting the biosynthetic pathway of L-lysine for antibiotic drug discovery, a considerable amount of research has been directed towards understanding the enzymes involved in the diaminopimelate (Dap) pathway. The aminotransferase enzyme involved in the Dap pathway (DapL) has previously been characterised in three different organisms, however it has never been characterised from the bacteria *Verrucomicrobium spinosum* [1-4]. *V. spinosum* has the unique feature of only using the aminotransferase pathway to synthesise L-lysine and its precursor *meso*-Dap, therefore it can be used as a model organism in the development of potential antibacterial, herbicidal or algaecidal compounds [5]. Expression and purification of the DapL protein from *V. spinosum* (*Vs*DapL), was required to understand its structural, biophysical and kinetic properties discussed in later chapters.

The work in this chapter includes the successful expression and purification of *Vs*DapL, using *Escherichia coli* in BL21*(DE3) cells. The pET30a(+) plasmid containing the His-Tagged *Vs*DapL gene was generously provided by Associate Professor André Hudson of Rochester Institute of Technology. Previously reported methods of expression and purification were adapted here for the best expression of *Vs*DapL.

2.2 Transformation and over-expression of *Vs*DapL

Escherichia coli expression strains are the favored bacterial expression system for heterologous gene expression due to the significant advantages including the feature of quick growth, simplicity and low cost [6, 7]. In this work, the BL21*(DE3) expression strain was used the in the initial transformations. BL21*(DE3) are a non-

T7 expression strain that has a mutation in the RNAseE gene, resulting in a greater transcript half-life [8]. The pET30a(+) plasmid containing the His-Tagged *Vs*DapL gene was transformed into BL21*(DE3) expression cells. Transformed colonies formed overnight on kanamycin containing agar pates and were used for expression. Previously reported methods were trialed *via* small-scale expression allowing the best conditions for *Vs*DapL to be established. The expression method that was found to be the best for over-expression of *Vs*DapL followed the protocol detailed in Chapter 6, section 6.3.7 and was used in all expression work throughout this thesis. Cells were harvested following protein expression via centrifugation and either frozen at -20°C for future use, or resuspended in appropriate buffer ready for lysis.

2.3 Cell lysis

There are several practices to lyse bacterial cells, however throughout this work cells were lysed using sonication via an ultrasonic probe. Sonication involves the shearing of cells by the immersion of a probe into the desired solution and emitting ultrasonic high frequency sound waves in pulses [9]. The cells were resuspended in appropriate buffer and were sheared open via sonication. In order to achieve maximum cell shearing, while limiting the denaturing of a protein, the temperature of the solution and time intervals between sonication was carefully monitored as heat is liberated in the process [10]. Shearing of the cells released the proteins within the cell into the suspension where it was then centrifuged to separate insoluble and soluble protein. Soluble proteins remained in the supernatant, while the insoluble proteins and other aggregates formed a pellet. The supernatant (or crude lysate) containing soluble *Vs*DapL was carefully collected and kept on ice or at 4°C ready for purification and the pellet was discarded.

2.4 Immobilised metal affinity chromatography (IMAC)

Following collection of the crude lysate, *Vs*DapL was purified by means of immobilised metal affinity chromatography (IMAC), whereby a polyhistidine tag on the protein chelates to Ni^{+} ions as it passes through the column [11]. The crude lysate

containing His-tagged *Vs*DapL was loaded onto the IMAC column, washed with buffer containing low imidazole to remove any nonspecific binding, and then eluted with buffer containing high imidazole. Purity of *Vs*DapL was assessed using SDS-PAGE (Figure 2.1).

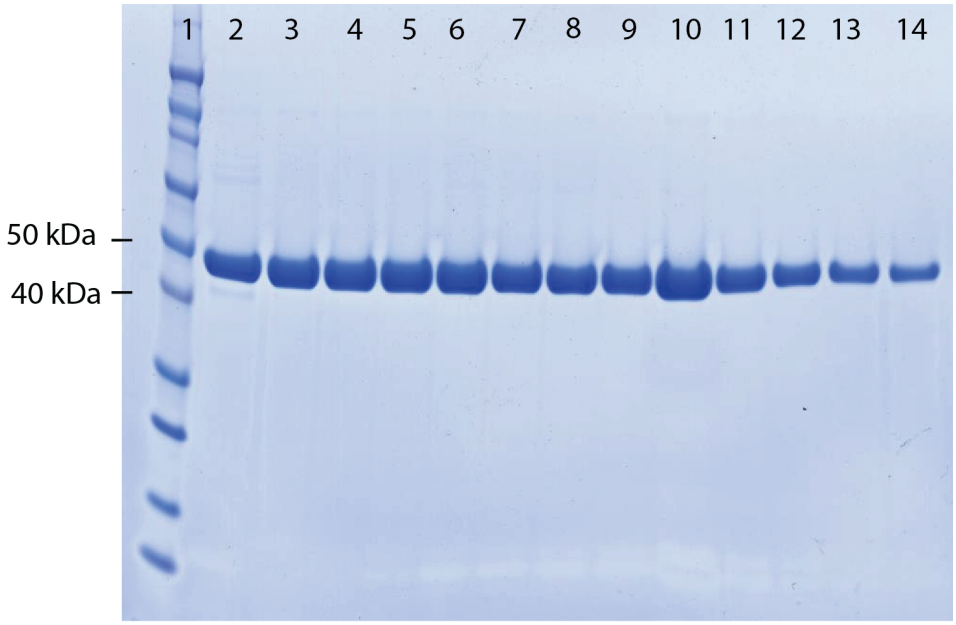

Figure 2.1: SDS-PAGE following the IMAC His-Trap Purification of *Vs*DapL:. Lanes 1: Protein Standard (Top to bottom (kDa): 160, 110, 80, 60, 50, 40 30, 20,15 and 10) Lanes 2-13 – eluted fractions

Comassie brilliant blue staining of the gel displayed a single band at approximately 45 kDa which is in agreement with the calculated molecular weight of *Vs*DapL as a monomer at 44.7 kDa, calculated from the amino acid sequence using exPASy ProtParam and beer's law [12]. The fractions containing *Vs*DapL were pooled and concentrated to a volume of 1.5 mL for further purification.

2.5 Size exclusion chromatography

Size exclusion chromatography (SEC) was used as a second purification step to separate proteins that may have co-eluted with *Vs*DapL in the IMAC purification step. Separation using SEC is based on the size of the molecule, as smaller molecules pass through a column containing specifically shaped small pores slower than larger molecules [13]. Pooled fractions from the IMAC purification step containing *Vs*DapL

were loaded onto a pre-equilibrated column and eluted over 120 minutes with desired buffer. Fractions were collected in 1 mL aliquots and purity of the *Vs*DapL was assessed using SDS-PAGE (figure 2.2). Comassie brilliant blue staining of the gel displayed a single band at approximately 44.7 kDa indicating pure *Vs*DapL.

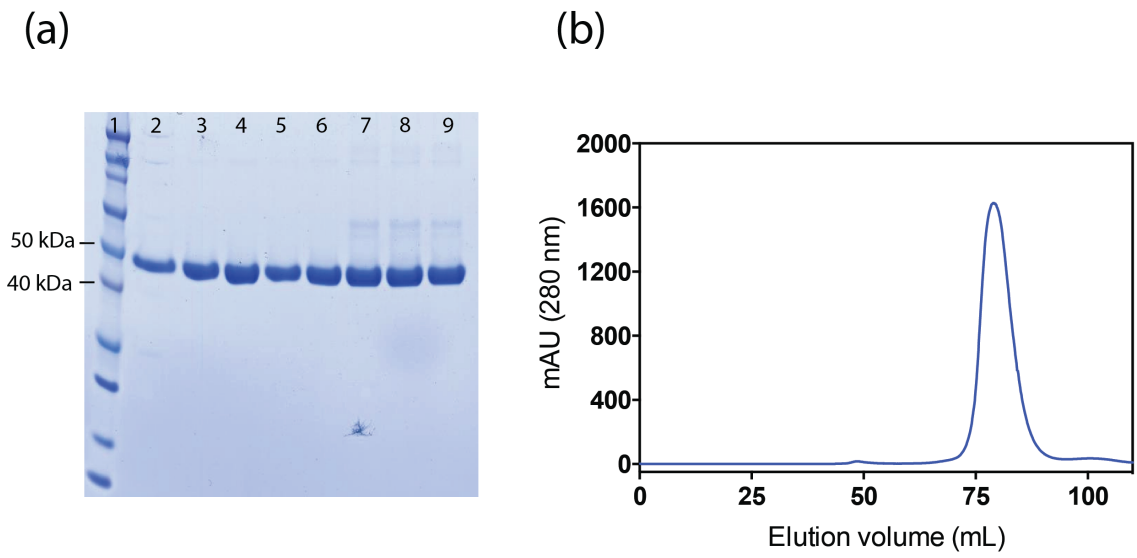

Figure 2.2: SEC purification of *Vs*DapL (a) An SDS-PAGE gel of collected fractions within the peak following SEC. Lane 1: Protein Standard (Top to bottom (kDa): 160, 110, 80, 60, 50, 40 30, 20,15 and 10), Lanes 2-9: fractions from the peak displayed by SEC chromatogram (b) SEC chromatogram displaying the elution of VsDapL.

Samples from each step of the purification were run on SDS-PAGE to track a typical purification of *Vs*DapL (figure 2.3). The protein became more pure with each purification step. The band at 44.7 kDa, indicative of the monomeric molecular weight of *Vs*DapL, becomes increasingly visible with less contamination following IMAC and SEC purification methods, however SEC was run in all purifications to remove any impurities that may have been present following IMAC. The concentration of the purified *Vs*DapL was calculated using a Nanodrop spectrophotometer or by the Bradford assay Pure protein was then pipetted into different volumes and concentration aliquots, snap frozen in liquid nitrogen and stored at -80 °C.

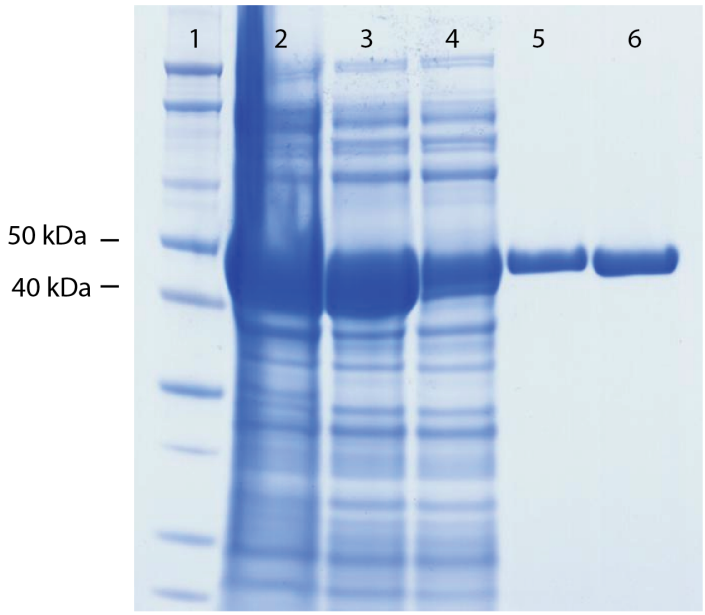

Figure 2.3: SDS-PAGE showing the purification process of *Vs*DapL. Lane 1: Protein Standard (Top to bottom (kDa): 110, 80, 60, 50, 40 30, 20,15 and 10), Lane 2, Crude lysate; Lane 3, Soluble protein (centrifuged lysate); Lane 4, IMAC flow through; Lane 5, Post IMAC; Lane 6, Post SEC.

Table 2.1 Purification table of a typical VsDapL purification

	Starting Volume	Crude lysate	Protein (mg/mL after IMAC)	Protein (mg/mL) after SEC
*Vs*DapL	2 L	~50 mL	1.5 mL at 35 mg/mL	1 mL at 20 mg/mL

2.6 Summary

In order to assess the biophysical, structural and kinetic properties, successful expression and purification of the *Vs*DapL was required. This chapter describes the transformation of *Vs*DapL into *E. coli* BL21*(DE3) cells, followed by the successful over-expression and purification via a two-step purification process with the use of IMAC and size exclusion chromatography. SDS Page gel electrophoresis was used to confirm the purity of *Vs*DapL after purification.

2.7 References

[1] Watanabe, N., Cherney, M. M., van Belkum, M. J., Marcus, S. L., Flegel, M. D., Clay, M. D., Deyholos, M. K., Vederas, J. C., and James, M. N. (2007) Crystal structure of LL-diaminopimelate aminotransferase from Arabidopsis thaliana: a recently discovered enzyme in the biosynthesis of L-lysine by plants and Chlamydia, *J Mol Biol 371*, 685-702.

[2] Dobson, R. C., Giron, I., and Hudson, A. O. (2011) L,L-diaminopimelate aminotransferase from Chlamydomonas reinhardtii: a target for algaecide development, *PLoS One 6*, e20439.

[3] Watanabe, N., Clay, M. D., van Belkum, M. J., Fan, C., Vederas, J. C., and James, M. N. (2011) The structure of LL-diaminopimelate aminotransferase from Chlamydia trachomatis: implications for its broad substrate specificity, *J Mol Biol 411*, 649-660.

[4] McCoy, A. J., Adams, N. E., Hudson, A. O., Gilvarg, C., Leustek, T., and Maurelli, A. T. (2006) L,L-diaminopimelate aminotransferase, a trans-kingdom enzyme shared by Chlamydia and plants for synthesis of diaminopimelate/lysine, *Proc Natl Acad Sci U S A 103*, 17909-17914.

[5] Triassi, A. J., Wheatley, M. S., Savka, M. A., Gan, H. M., Dobson, R. C., and Hudson, A. O. (2014) L,L-diaminopimelate aminotransferase (DapL): a putative target for the development of narrow-spectrum antibacterial compounds, *Front Microbiol 5*, 509.

[6] Fathi-Roudsari, M., Akhavian-Tehrani, A., and Maghsoudi, N. (2016) Comparison of Three Escherichia coli Strains in Recombinant Production of Reteplase, *Avicenna J Med Biotechnol 8*, 16-22.

[7] Terpe, K. (2006) Overview of bacterial expression systems for heterologous protein production: from molecular and biochemical fundamentals to commercial systems, *Appl Microbiol Biotechnol 72*, 211-222.

[8] Wang, H., Wang, F., Wang, W., Yao, X., Wei, D., Cheng, H., and Deng, Z. (2014) Improving the expression of recombinant proteins in E. coli BL21 (DE3) under acetate stress: an alkaline pH shift approach, *PLoS One 9*, e112777.

[9] Brown, R. B., and Audet, J. (2008) Current techniques for single-cell lysis, *J R Soc Interface 5 Suppl 2*, S131-138.

[10] Kwon, Y. C., and Jewett, M. C. (2015) High-throughput preparation methods of crude extract for robust cell-free protein synthesis, *Sci Rep 5*, 8663.

[11] Robichon, C., Luo, J., Causey, T. B., Benner, J. S., and Samuelson, J. C. (2011) Engineering Escherichia coli BL21(DE3) derivative strains to minimize E. coli protein contamination after purification by immobilized metal affinity chromatography, *Appl Environ Microbiol 77*, 4634-4646.

[12] Wilkins, M. R., Gasteiger, E., Bairoch, A., Sanchez, J. C., Williams, K. L., Appel, R. D., and Hochstrasser, D. F. (1999) Protein identification and analysis tools in the ExPASy server, *Methods Mol Biol 112*, 531-552.

[13] Hong, P., Koza, S., and Bouvier, E. S. (2012) Size-Exclusion Chromatography for the Analysis of Protein Biotherapeutics and their Aggregates, *J Liq Chromatogr Relat Technol 35*, 2923-2950.

Chapter Three - Kinetic Analysis of *Vs*DapL

3.1 Introduction

As outlined in chapter one chapter 1, the diaminopimelate (Dap) pathway provides an alternative route to L-lysine, as it catalyses a reaction that bypasses several enzymatic steps. Previously reported catalytic mechanisms for pyridoxal-5-phosphate (PLP) dependent aminotransferase enzymes show that the reaction follows the bimolecular ping-pong mechanism and is, of course, reversible (Figure 3.1) [1, 2].

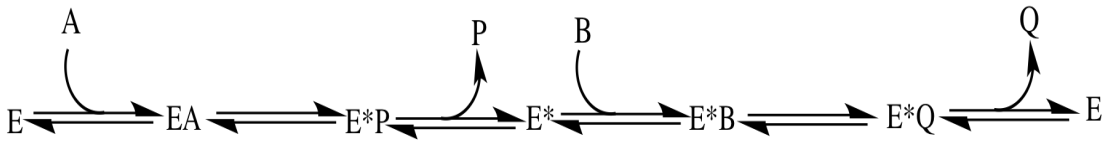

Figure 3.1: The general mechanism scheme of ping-pong bimolecular reactions. E = enzyme , A= substrate 1 , EA enzyme substrate 1 complex, E*P= modified enzyme product complex, E* = modified enzyme, E*B enzyme substrate 2 complex, E*Q = modified enzyme product 2 complex, Q = Product 2.

In the transaminase reaction, an amino-group is transferred from an amino donor (usually an amino acid) to its corresponding α-keto acid, which acts as an amino acceptor [3]. A general schematic of the role of PLP in a typical aminotransferase reaction mechanism is shown below in Figure 3.2. The mechanism proceeds through the formation of a Schiff base, whereby PLP acts as a co-enzyme and is tethered to a lysine side chain located within the active site of the enzyme [4, 5]. This allows the amine group to be donated onto the keto- moiety of the amino acceptor to form it's conjugate amino acid [6].

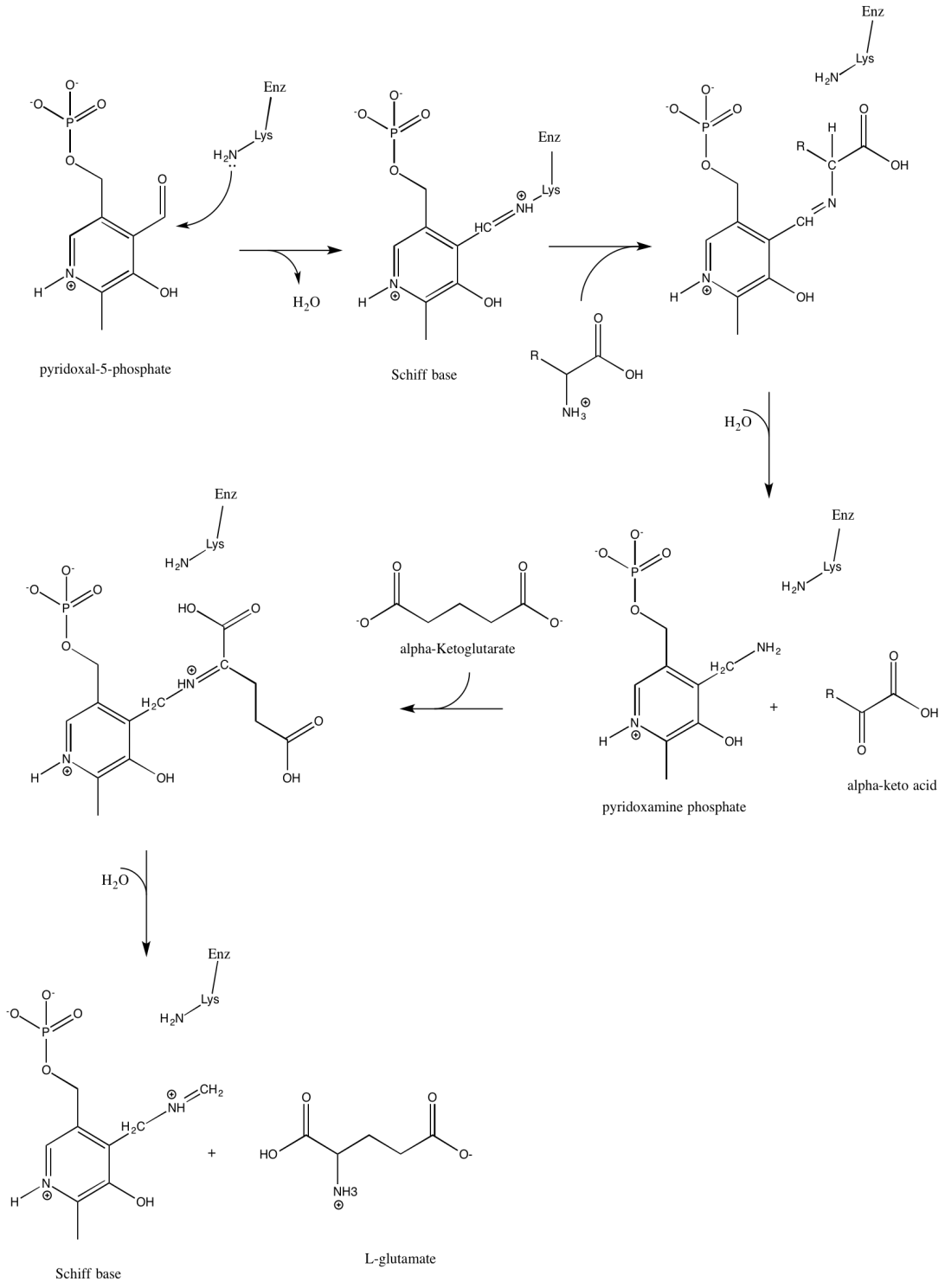

Figure 3.2: The proposed reaction catalysed by transaminases. Taken from [7] and adapted in CHEMDRAW.

3.2 The aminobenzaldehyde assay

The aminobenzaldehyde assay has previously been developed to collect initial rate data of PLP-dependent aminotransferase enzymes. It measures the initial rate of the reaction, whereby a change in concentration of either substrate or product is measured as a function of time [8]. A variation of the aminobenzaldehyde assay, the coupled *ortho*-aminobenzaldehyde assay developed by Hudson et al. 2006 [9], measures the production of a dihydroquinazolium adduct at 440 nanometers (nm) and has been reported in several diaminopimelate aminotransferase (DapL) kinetic studies [10-13]. In this work, the catalytic activity of *Verrucomicrobium spinosum* DapL (*Vs*DapL) was measured using this assay in the reverse direction (Figure 3.3).

The forward (anabolic) reaction proceeds via the donation of an amine group from L-glutamate to tetrahydrodipicolinate acid (THDP), while in the reverse (catabolic) reaction the amine group from L,L-diaminopimelate is donated onto α-ketoglutarate (α-KG) [14]. *o*-Aminobenzaldehyde reacts with THDP and generates a yellow tinted dihydroquinazolium adduct that absorbs light at 440 nm. The activity of the *o*-aminobenzaldehyde assay has been noted to proceed significantly faster via the reverse direction with respect to the kinetic parameter V_{max} [10]. The side reaction that may occur between α-ketoglutarate and *o*-aminobenzaldehyde has been shown to be so poor that it can be considered negligible, thus this coupled assay provides a simple yet practical method for the determination of initial rate [15].

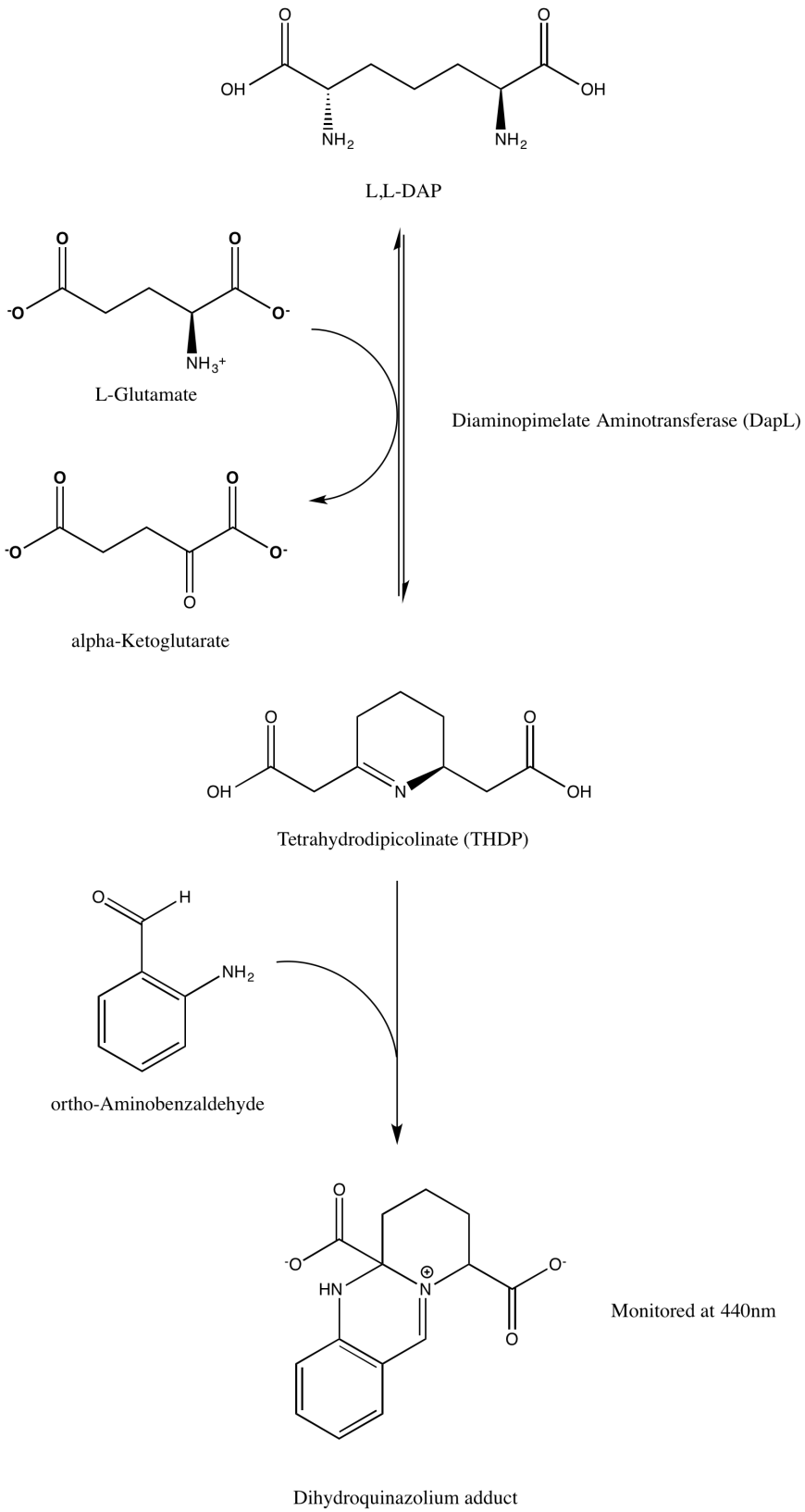

Figure 3.3: The chemical reaction scheme of the variation of *o*-aminobenzaldehyde Assay. The formation of THDP is coupled to the formation of a dihydroquinazolium adduct that absorbs at 440 nm. Figure generated in CHEMDRAW.

3.3 *Vs*DapL *o*-aminobenzaldehyde assay

The reverse *o*-aminobenzaldehyde was used to extrapolate kinetic parameters of *Vs*DapL. The assay showed that *Vs*DapL is a reasonably inefficient enzyme with respect to the substrate L,L Dap. The apparent values for K_M (4.1 mM) and V_{max} (0.52 mM/s^{-1}) are consistent with those previously reported in the literature (Table 3.1). However, the catalytic turnover rate of 7.7 s^{-1} and the catalytic efficiency 1.9 x 10^3 $s^{-1}M^{-1}$ measured for *Vs*DapL are slightly higher than previously reported values but are still notably lower than other reported DapL orthologues [16].

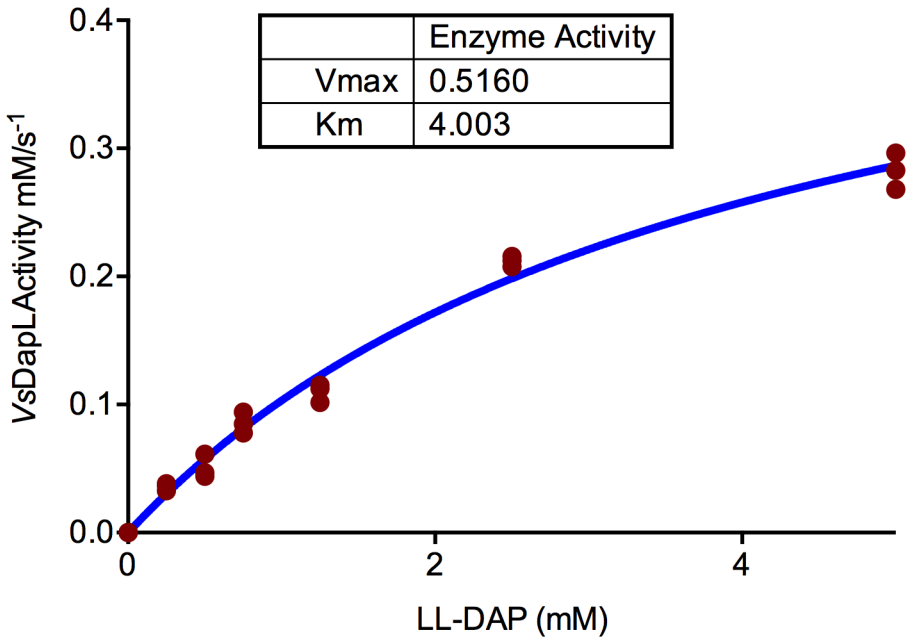

Figure 3.4: Kinetic plot showing the activity of *Vs*DapL against varying concentrations of substrate (L,L-Dap) at pH 7.0. A Michaelis-Menten curve was fitted to find the kinetic parameters Km and Vmax. Data was fitted using Prism 6

Table 3.1: Kinetic parameters for the *o*-aminobenzaldehyde assay with *Vs*DapL. Previously reported constants for VsDapL* and CrDapL are compared.

	*Vs*DapL	*Vs*DapL*	*Cr*DapL
K_M for L,L Dap (mM)	4.003 ± 0.4	4.1± 1	2.7± 0.7
k_{cat} (s^{-1})	7.719	1.6	16.4
k_{cat} / K_m ($s^{-1}M^{-1}$)	1.9 x 10^3	0.4 x 10^3	6.1 x 10^3

3.4 *Vs*DapL *ortho*-aminobenzaldehyde inhibition assay

As DapL orthologues have potential to be used in the development of antibacterial, herbicide or algaecide compounds, a number of inhibitors have been screened with the enzyme [14, 16]. The inhibitors identified in the initial screens (malic/maleic acid) were required in elucidating the crystal structure of *Vs*DapL (Chapter five); therefore it was logical to attempt to determine catalytic properties of *Vs*DapL in the presence of these inhibitors.

Three models of inhibition (competitive, mixed and non-competitive) were fitted to the inhibition assay experimental data. When modeled, the data did not fit any of the models, however mixed inhibition provided the closest fit (Figure 3.5).

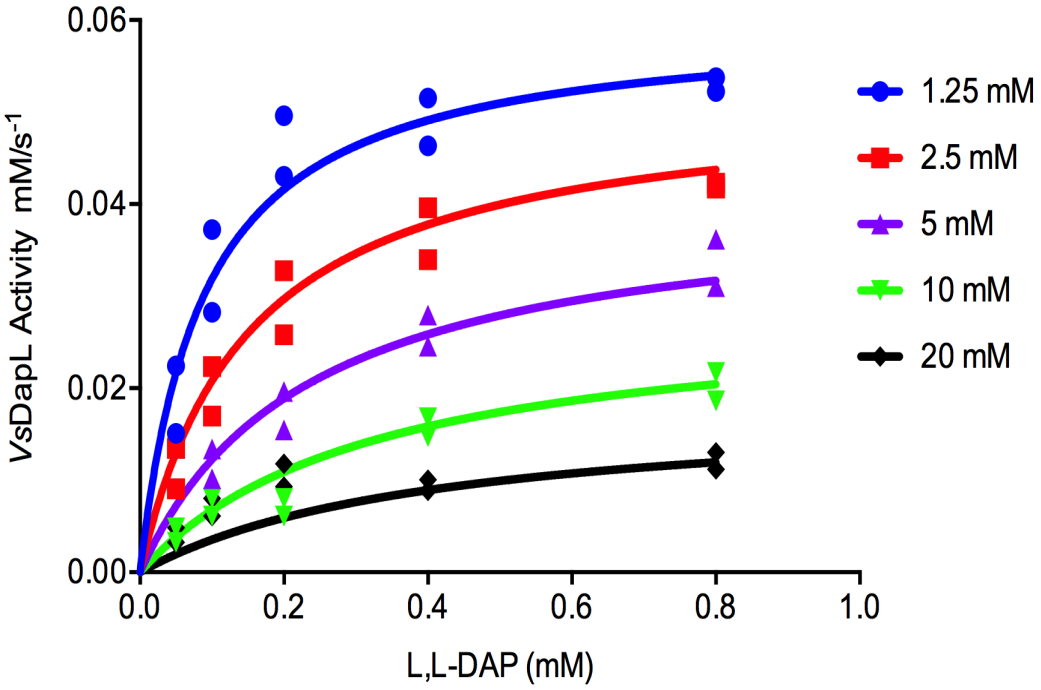

Figure 3.5: Kinetic plot showing the activity of *Vs*DapL against varying concentrations of substrate (L,L-Dap) with varying concentrations of inhibitor (Malic acid) present at pH 7.0. A mixed-inhibition fit was modeled to the experimental data and graphed using Prism 6.

A Lineweaver-Burk plot was generated to determine the model that best describes the experimental data (Figure 3.6). If the data were to fit a competitive inhibition model then only the K_M would increase as the inhibitor concentration increased while Vmax would remain the same. In the noncompetitive model, the V_{max} would increase as the concentration of inhibitor increased, while K_M remains constant. From the experimental data, it can be seen that both V_{max} and K_M are clearly altered by an increase in inhibitor concentration and therefore the mixed inhibition model was fitted. The apparent inhibition constant (K_I) of 48.7 µM was calculated from the mixed-inhibition model. R-square values given from each model were also compared and best fitted mixed inhibition.

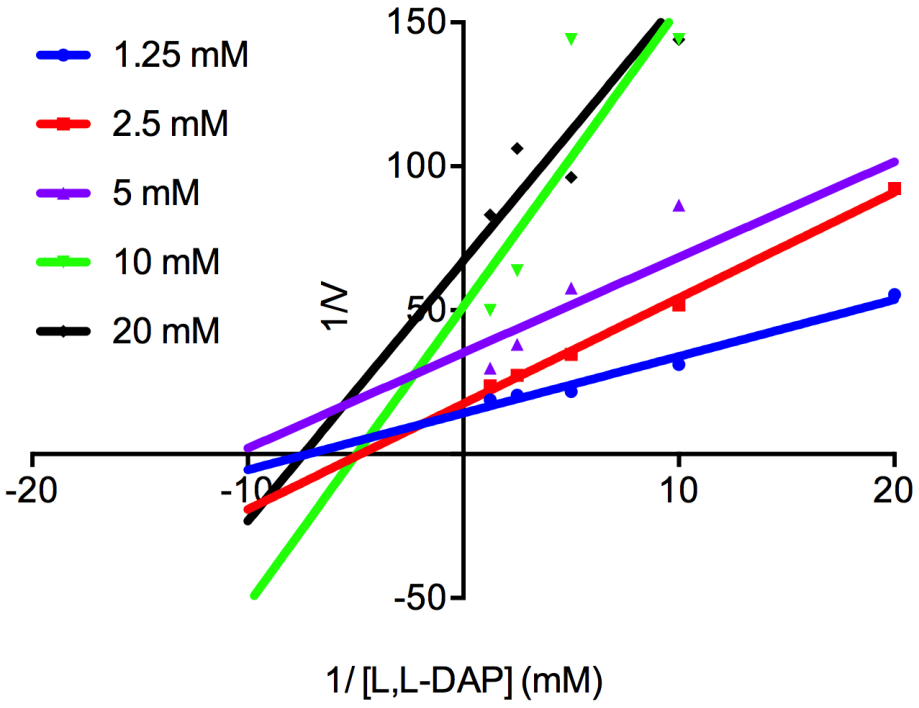

Figure 3.6: A Lineweaver-Burk plot showing the activity of *Vs*DapL against varying concentrations of substrate (L,L-Dap) with varying concentrations of inhibitor (Malic acid) present at pH 7.0. A mixed-model inhibition fit was modeled to the experimental data and graphed using Prism 6.

3.4 Summary

The reverse coupled *o*-aminobenzaldehyde was used to extrapolate kinetic parameters of *Vs*DapL. The apparent values for the K_M of 4.1 mM and V_{max} 0.52 mM/s^{-1} were calculated using prism and were consistent to previously reported values. Inhibition assays were set up, however a model of inhibition could not be completely fitted to the data. A mixed-inhibition provided the closest fit and a K_I of 48.7 μM was calculated.

3.5 References

[1] Triassi, A. J., Wheatley, M. S., Savka, M. A., Gan, H. M., Dobson, R. C., and Hudson, A. O. (2014) L,L-diaminopimelate aminotransferase (DapL): a putative target for the development of narrow-spectrum antibacterial compounds, *Front Microbiol 5*, 509.

[2] Velick, S. F., and Vavra, J. (1962) A kinetic and equilibrium analysis of the glutamic oxaloacetate transaminase mechanism, *J Biol Chem 237*, 2109-2122.

[3] Cassimjee, K. E., Manta, B., and Himo, F. (2015) A quantum chemical study of the omega-transaminase reaction mechanism, *Org Biomol Chem 13*, 8453-8464.

[4] Alexander, F. W., Sandmeier, E., Mehta, P. K., and Christen, P. (1994) Evolutionary relationships among pyridoxal-5′-phosphate-dependent enzymes, *European Journal of Biochemistry 219*, 953-960.

[5] Jahn, D., Chen, M. W., and Soll, D. (1991) Purification and functional characterization of glutamate-1-semialdehyde aminotransferase from *Chlamydomonas reinhardtii*, *J Biol Chem 266*, 161-167.

[6] Liepman, A. H., and Olsen, L. J. (2004) Genomic Analysis of Aminotransferases in *Arabidopsis thaliana*, *Critical Reviews in Plant Sciences 23*, 73-89.

[7] Dajnowicz, S., Johnston, R. C., Parks, J. M., Blakeley, M. P., Keen, D. A., Weiss, K. L., Gerlits, O., Kovalevsky, A., and Mueser, T. C. (2017) Direct visualization of critical hydrogen atoms in a pyridoxal 5′-phosphate enzyme, *Nature Communications 8*, 955.

[8] Waley, S. G. (1981) An easy method for the determination of initial rates, *Biochem J 193*, 1009-1012.

[9] Hudson, A. O., Singh, B. K., Leustek, T., and Gilvarg, C. (2006) An LL-diaminopimelate aminotransferase defines a novel variant of the lysine biosynthesis pathway in plants, *Plant Physiol 140*, 292-301.

[10] Hudson, A. O., Gilvarg, C., and Leustek, T. (2008) Biochemical and phylogenetic characterization of a novel diaminopimelate biosynthesis pathway in prokaryotes identifies a diverged form of LL-diaminopimelate aminotransferase, *J Bacteriol 190*, 3256-3263.

[11] Dobson, R. C., Giron, I., and Hudson, A. O. (2011) L,L-diaminopimelate aminotransferase from *Chlamydomonas reinhardtii:* a target for algaecide development, *PLoS One 6*, e20439.

[12] Toyama, S., Yasuda, M., Miyasato, K., Hirasawa, T., and Soda, K. (1974) A new assay method of .OMEGA.-amino acid aminotransferase with *o*-aminobenzaldehyde, Vol. 38.

[13] McCoy, A. J., Adams, N. E., Hudson, A. O., Gilvarg, C., Leustek, T., and Maurelli, A. T. (2006) L,L-diaminopimelate aminotransferase, a trans-kingdom enzyme shared by Chlamydia and plants for synthesis of diaminopimelate/lysine, *Proc Natl Acad Sci U S A 103*, 17909-17914.

[14] Triassi, A. J., Wheatley, M. S., Savka, M. A., Gan, H. M., Dobson, R. C. J., and Hudson, A. O. (2014) L,L-diaminopimelate aminotransferase (DapL): a putative target for the development of narrow-spectrum antibacterial compounds, *Frontiers in Microbiology 5*, 509.

[15] Soda, K., Toyama, S., Misono, H., Hirasawa, T., and Asada, K. (1973) Spectrophotometric Determination of Glyoxylic Acid with o-Aminobenzaldehyde and Glycine, and Its Application to Enzyme Assay, *Agricultural and Biological Chemistry 37*, 1393-1400.

[16] McKinnie, S. M., Rodriguez-Lopez, E. M., Vederas, J. C., Crowther, J. M., Suzuki, H., Dobson, R. C., Leustek, T., Triassi, A. J., Wheatley, M. S., and Hudson, A. O. (2014) Differential response of orthologous L,L-diaminopimelate aminotransferases (DapL) to enzyme inhibitory antibiotic lead compounds, *Bioorg Med Chem 22*, 523-530.

Chapter Four - Biophysical Characterisation of *Vs*DapL

4.1 Introduction

To assist X-ray crystallography and nuclear magnetic resonance structural studies, a range of biophysical techniques are available to probe the biological function of a protein [1, 2]. These cover areas including hydrodynamics, thermodynamics and spectroscopy to uncover the properties of a protein in solution. As diaminopimelate aminotransferase (DapL) is a recently discovered enzyme, limited information is known about its structural characteristics, therefore biophysical techniques could aid the elucidation of its properties [3]. In this chapter, the biophysical properties of *Verrucomicrobium spinosum* DapL (*Vs*DapL) were explored using three techniques, circular dichroism spectroscopy (CD), analytical ultracentrifugation (AUC) and small angle X-ray scattering (SAXS). These techniques provide invaluable insight into the size, shape and structure of *Vs*DapL in solution.

4.2 Circular dichroism

Circular dichroism spectroscopy is a biophysical technique that measures the difference in absorption of left-handed and right-handed circular polarised light [4]. Peptide bonds of proteins absorb in the far-UV region of 180-240 nanometers (nm) and therefore CD is primarily used for the evaluation of the secondary structure composition, folding and binding properties of a protein [5, 6]. α-Helices give a characteristic positive single peak at 193 nm and two negative peaks at 208 and 222 nm on a CD spectrum, while β-sheets give a single positive peak at 195 nm and a single negative peak at 218 nm [5]. The secondary structure elements of *Vs*DapL were analysed using a wavelength-scan in the far-UV region (between 190-260 nm). The thermal denaturation of *Vs*DapL was also measured using CD, however two other techniques, differential scanning calorimetry and differential scanning fluorimetry were used prior to analysis with CD. Both techniques gave inconclusive results and therefore CD was used as the primary method for gauging the thermal properties of *Vs*DapL.

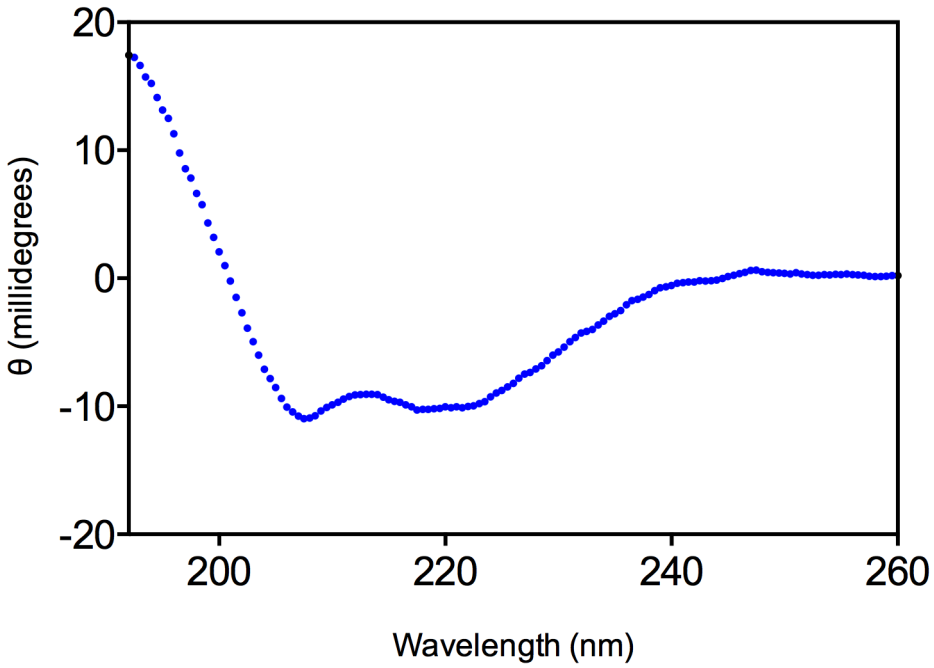

Figure 4.1 – Far-UV CD spectrum of *Vs*DapL at 0.1 mg/mL in 50 mM Tris-HCl buffer, 150 mM NaCl (pH 7.6) in a 2mm cuvette. The spectrum was collected between 190-260 nm and the mean residue ellipticity θ, was plotted against wavelength in nm.

An initial wavelength scan between 190 and 260 nm resulted in a spectrum displayed two negative peaks at approximately 208 nm and 222 nm (Figure 4.1). These peaks indicate that *Vs*DapL was folded in solution and contained a proportion of both α-helices and β-sheets.

A thermal denaturation profile for *Vs*DapL was obtained at 220 nm by heating the sample from 20°C to 95°C and taking measurements at 0.3°C increments. The mean residue ellipticity θ was plotted as a function of temperature and is shown in (Figure 4.2). The corresponding sigmoidal curve given denotes the thermal denaturation profile of *Vs*DapL and by locating the midpoint of the transition, the melting temperature was calculated to be approximately 51°C. Wavelength scans were also taken at between 190 and 260 nm at 10°C increments to visualise the denaturation of *Vs*DapL (Figure 4.3).

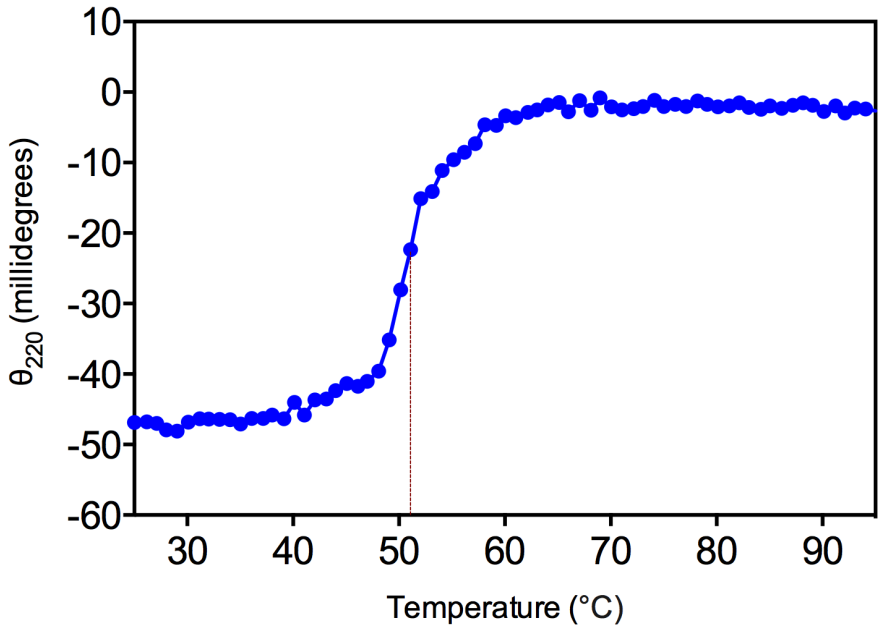

Figure 4.2 – The thermal denaturation profile of *Vs*DapL in 0.1 mg/mL in 50 mM Tris-HCl buffer, 150 mM NaCl (pH 7.6) in a 2 mm cuvette. Mean residue ellipticity [θ] at 220 nm is plotted against temperature and the thermal denaturation temperature is shown in red.

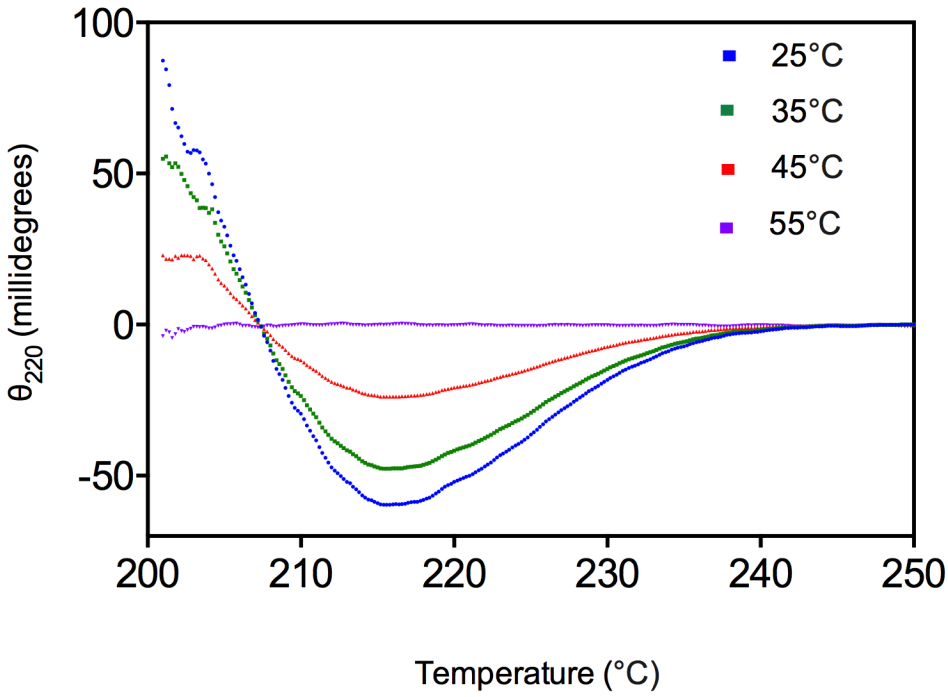

Figure 4.3 – The overlay of the Far-UV CD spectra of *Vs*DapL in 0.1 mg/mL in 50 mM Tris-HCl buffer, 150 mM NaCl (pH 7.6) in a 2mm cuvette. Collected spectra were taken at 10°C increments between 190-260 nm and the mean residue ellipticity θ, was plotted against wavelength in nm. Measurements above 55°C where *Vs*DapL was unfolded were omitted from the overlay.

4.3 Analytical ultracentrifugation

Analytical ultracentrifugation (AUC) is a powerful and versatile method for the quantitative characterisation of macromolecule associations in solution [7, 8]. There are two experimental designs in AUC, sedimentation velocity, where the sedimentation process is the focus, and sedimentation equilibrium where the final equilibrium distribution is analysed [9, 10]. Both techniques can provide useful information about thermodynamic and hydrodynamic properties of a macromolecule in solution. In this work, the sedimentation velocity experiment was used to assess the oligomeric state of *Vs*DapL in solution. The experiment measures the rate at which molecules move in response to an applied centrifugal force, as a function of time, and therefore allows conclusions about its size and shape in solution [11, 12].

As displayed in the three previously reported crystal structures, DapL adopts a homo-dimeric structure (See chapter 1, section 1.4). It was reasoned that *Vs*DapL should also adopt a dimeric oligomeric state, however to examine if there was a concentration dependence on the oligomeric state, *Vs*DapL was tested at three different concentrations using sedimentation velocity.

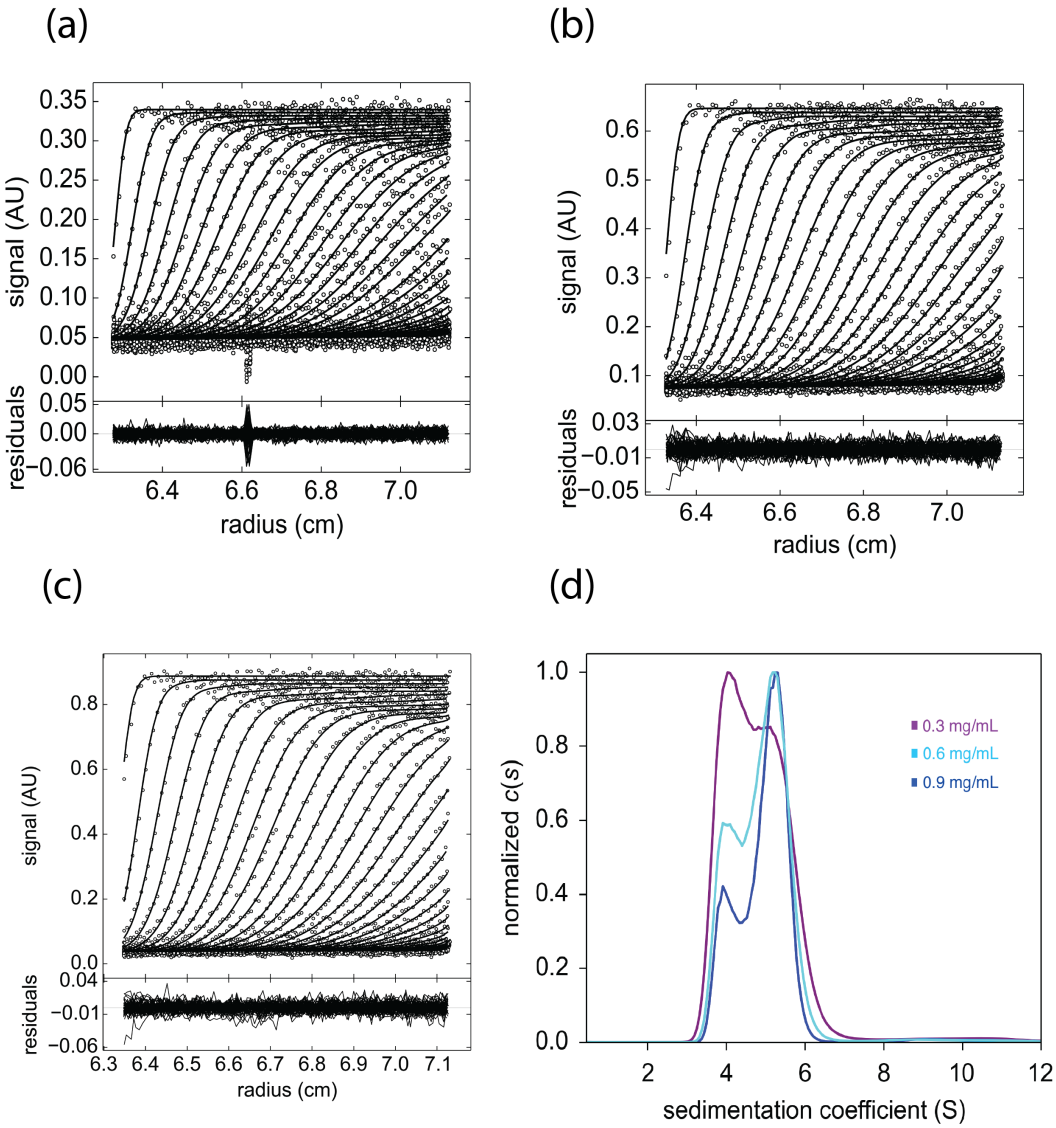

Figure 4.4: Analytical ultracentrifugation sedimentation velocity of *Vs*DapL carried out at three concentrations in 20 mM Tris-HCl, 150mM NaCl, pH 7.6 20ºC. (a) The sedimentation velocity of *Vs*DapL at 0.3 mg/mL with the residuals for nonlinear least squares fit plotted. (b) The sedimentation velocity of *Vs*DapL at 0.6 mg/mL with the residuals for nonlinear least squares fit plotted. (c) The sedimentation velocity of *Vs*DapL at 0.9 mg/mL with the residuals for nonlinear least squares fit plotted. (d) An overlay of the continuous sedimentation coefficient c(s) distribution for all three concentrations plotted as a function of the sedimentation coefficient.

Table 4.1: Calculated AUC parameters for *Vs*DapL.

	0.3 mg/mL	0.6 mg/mL	0.9 mg/mL
Weight averaged c (s), $S_{20,w}$	4.67	4.83	4.87
RMSD	0.006917	0.006672	0.007286
Runs test z score	1.57	6.76	9.78
f/f_0	1.016	1.079	1.106

Sedimentation velocity data was fitted to a c(s) model and at the lowest concentration of 0.3 mg/mL, the c(s) plot displays peaks corresponding to sedimentation coefficients of approximately 4 and 6 S (Figure 4.4, d). The program, HydroPRO, was used to estimate the sedimentation coefficient for the dimeric structure of *Vs*DapL from the molecular model (Chapter 5), and was calculated to be 5.73 S, consistent with the value of approximately 6 S given in the experiment. The lower 4 S peak corresponds to a monomer, and is shown to be at higher ratio than the 6 S peak, indicating that a higher proportion of monomer than dimer is present at this concentration. The quality of the nonlinear least squares best-fit is supported by the low root-mean-square deviation (RMSD) number of 0.006917 (Table 4.1), and the random residual distribution show normally distributed noise (Figure 4.4, a). The spike located on the residuals plot at just above 6.6 cm can be attributed to a scratch located on the cell that was used for the SV experiment at this concentration.

At the concentration of 0.6 mg/mL the c(s) plot displays peaks corresponding to sedimentation coefficients of approximately 4 and 6 S (Figure 4.4, d). However, the c(s) peaks are different compared to the lower concentration indicating that the solution contains a higher proportion of dimer to monomer at this concentration. The quality of the nonlinear least squares best-fit is supported by the low RMSD number of 0.006672 and the random residual distribution show normally distributed noise (Table 4.1, b).

At the final tested concentration of 0.9 mg/mL, the c(s) plot again displays two peaks at the same sedimentation coefficients as prior (Figure 4.4, d). The c(s) peak at around 6 S is higher than that at 4 S and suggests that the dimeric species of *Vs*DapL comprises the majority of the solution, however a small proportion of monomer is still apparent. The RMSD of 0.007286 (Table 4.1), and the random residual distribution showing normally distributed noise indicated the quality of the nonlinear least squares best-fit (Figure 4.4, c).

The shift from a higher proportion of monomeric species at the lower concentrations, to a dimeric species at the higher concentrations examined here has not been reported for any of the previously characterised DapL. This finding suggests that the

dissociation constant (K_d) for *Vs*DapL to between the ranges of 0.3 mg/mL-0.9 mg/mL.

4.4 Small angle X-ray scattering

Following the previously unreported finding that the concentration of *Vs*DapL could affect its oligomeric state in solution, the biophysical technique small angle X-ray scattering (SAXS) was used. SAXS is used for the structural characterisation of a protein in solution, and therefore can offer unique insight into functionally important conformational changes under physiologically relevant conditions [13]. In this work, SAXS was used to complement the data obtained for *Vs*DapL from AUC.

SAXS data were collected at the Australian Synchrotron at SAXS/WAXS beamline and the scattering profiles were collected using the ATSAS package (Figure 4.5) [14]. Parameters for SAXS data analysis are given in Table 4.2.

The R_g against $I(0)$ as a function of time plot shows that the R_g value (red) is stable across these $I(0)$ values, indicating a monodisperse solution (Figure 4.5, a). The theoretical scattering profile from the dimeric crystal structure (chapter 5) is in close agreement with the experimental scattering model with a chi^2_{value} of 0.142 given from SREFLEX [15] (Figure 4.5, b). The Guinier plot, overlaid on the scattering profile also indicates that the sample does not show any indication of aggregation or inter-particle interference. The bell shaped nature of the Kratky plot shows that the *Vs*DapL is folded in solution (Figure 4.5, c). The maximum dimension of the particle (D_{max}) calculated from the p(r) plot of 96 Å attained from SAXS, is in close agreement with 96.1 Å measured for the dimeric crystal structure in Pymol, indicating that the enzyme is present as a dimer (Figure 4.5, d). AUC values for the dimeric molecular weight are consistent with dimeric values that are calculated from SAXS.

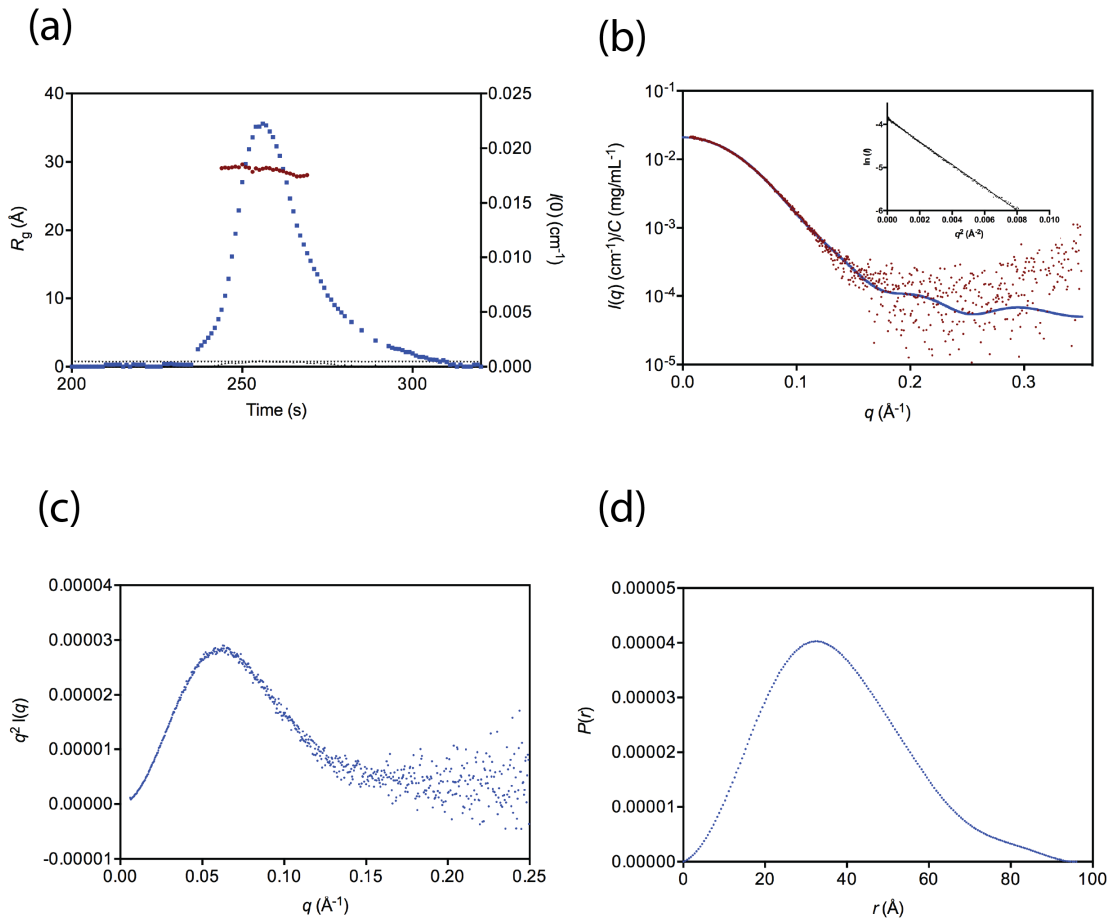

(b)

Figure 4.5: SEC-SAXS results for *Vs*DapL. (a) Plots showing $I(0)$ and Rg as a function of time for the SEC-SAXS run. (b) $I(q)$ versus q. Theoretical scattering of *Vs*DapL was fitted using SREFLEX. A Guinier plot is shown as an insert. (c) Kratky plot for the data in (b). (d) Pairwise distribution plot or P(r) .

Table 4.2: SAXS structural parameters of VsDapL

	*Vs*DapL
- Guinier analysis	
$I(0)$ (cm^{-1})	0.02
Rg (Å)	29.15
R^2	0.9986
chi^2	1.142
- P(r) analysis	
$I(0)$ (cm^{-1})	0.02
Rg (Å)	29.15
d_{max} (Å)	96
q range ($Å^{-1}$)	0.01-0.3
Porod volume ($Å^{-3}$)	112000.00
Calculated molecular weight	70,000
from Prorod volume (Da)	
- SAXS MoW analysis	
Molecular weight	3,883 Da
Number of chains	2

4.5 Summary

In this chapter three techniques, each designed to ascertain aspects relating to different biophysical properties, were used to paint an overall picture of *Vs*DapL in solution that could be used to complement X-ray crystallography studies. Circular dichroism spectroscopy was used as a tool to give insight into the secondary structure and thermodynamic properties of *Vs*DapL. It was found that the protein backbone contains both α-helices and β-sheets and when heated, the melting temperature was calculated to be approximately 51°C.

Analytical ultracentrifugation was used to investigate the oligomeric state of *Vs*DapL in solution. The identified feature of concentration dependent monomer-dimer equilibrium of *Vs*DapL in solution was found. At lower concentrations a higher proportion of the monomeric species was present, but as the concentration increased a higher proportion of dimeric species were observed. This finding suggests that the dissociation constant (K_d) of the *Vs*DapL monomer-dimer equilibrium to be in the range of 0.3-0.9 mg/mL.

Following AUC, Small angle X-ray scattering was used to investigate the size and shape of *Vs*DapL. SAXS samples were folded in solution with no signs of interparticle interference or aggregation and displayed a maximum particle size of 96 Å, consistent to what was found for a dimeric species in Pymol. The theoretical scattering profile calculated from the dimeric crystal structure of *Vs*DapL was in close agreement with the experimental scattering profile and thus further supports the dimeric structure in solution at higher concentrations. The biophysical data presented here was used to complement X-ray crystallography studies in the following chapter.

4.5 References

[1] Neet, K. E., and Lee, J. C. (2002) Biophysical characterization of proteins in the post-genomic era of proteomics, *Mol Cell Proteomics 1*, 415-420.

[2] Eliezer, D. (2009) Biophysical characterization of intrinsically disordered proteins, *Curr Opin Struct Biol 19*, 23-30.

[3] Nachar, V. R., Savka, F. C., McGroty, S. E., Donovan, K. A., North, R. A., Dobson, R. C., Buckley, L. J., and Hudson, A. O. (2012) Genomic and Biochemical Analysis of the Diaminopimelate and Lysine Biosynthesis Pathway in *Verrucomicrobium spinosum*: Identification and Partial Characterization of L,L-Diaminopimelate Aminotransferase and UDP-N-Acetylmuramoylalanyl-D-glutamyl-2,6-meso-Diaminopimelate Ligase, *Front Microbiol 3*, 183.

[4] Kelly, S. M., Jess, T. J., and Price, N. C. (2005) How to study proteins by circular dichroism, *Biochim Biophys Acta 1751*, 119-139.

[5] Greenfield, N. J. (2006) Using circular dichroism spectra to estimate protein secondary structure, *Nature protocols 1*, 2876-2890.

[6] Sklepari, M., Rodger, A., Reason, A., Jamshidi, S., Prokes, I., and Blindauer, C. A. (2016) Biophysical characterization of a protein for structure comparison: methods for identifying insulin structural changes, *Analytical Methods 8*, 7460-7471.

[7] Cole, J. L., Lary, J. W., T, P. M., and Laue, T. M. (2008) Analytical ultracentrifugation: sedimentation velocity and sedimentation equilibrium, *Methods Cell Biol 84*, 143-179.

[8] Howlett, G. J., Minton, A. P., and Rivas, G. (2006) Analytical ultracentrifugation for the study of protein association and assembly, *Curr Opin Chem Biol 10*, 430-436.

[9] Zhao, H., Brautigam, C. A., Ghirlando, R., and Schuck, P. (2013) Overview of current methods in sedimentation velocity and sedimentation equilibrium analytical ultracentrifugation, *Curr Protoc Protein Sci Chapter 20*, Unit20 12.

[10] Zhao, H., and Schuck, P. (2015) Combining biophysical methods for the analysis of protein complex stoichiometry and affinity in SEDPHAT, *Acta Crystallogr D Biol Crystallogr 71*, 3-14.

[11] Lebowitz, J., Lewis, M. S., and Schuck, P. (2002) Modern analytical ultracentrifugation in protein science: a tutorial review, *Protein Sci 11*, 2067-2079.

[12] Balbo, A., Minor, K. H., Velikovsky, C. A., Mariuzza, R. A., Peterson, C. B., and Schuck, P. (2005) Studying multiprotein complexes by multisignal sedimentation velocity analytical ultracentrifugation, *Proc Natl Acad Sci U S A 102*, 81-86.

[13] Skou, S., Gillilan, R. E., and Ando, N. (2014) Synchrotron-based small-angle X-ray scattering (SAXS) of proteins in solution, *Nature protocols 9*, 1727-1739.

[14] Konarev, P. V., Volkov, V. V., Sokolova, A. V., Koch, M. H. J., and Svergun, D. I. (2003) PRIMUS: a Windows PC-based system for small-angle scattering data analysis, *Journal of Applied Crystallography 36*, 1277-1282.

[15] Panjkovich, A., and Svergun, D. I. (2016) Deciphering conformational transitions of proteins by small angle X-ray scattering and normal mode analysis, *Phys Chem Chem Phys 18*, 5707-5719.

Chapter Five - The crystal structure of DapL from *Verrucomicrobium spinosum*

5.1 Introduction

X-ray crystallography is a powerful technique used to determine the atomic three-dimensional structure of a protein or macromolecule [1]. The atomic structure can be used to give detailed insights into the dynamics, interactions and function of a protein [2, 3]. In an effort to further characterise the diaminopimelate aminotransferase enzyme from *Verrucomicrobium spinosum* (*Vs*DapL), X-ray crystallography was used to elucidate the crystal structure. As outlined in chapter one, the first published crystal structure of DapL was solved in from the plant *A. thaliana* and subsequent studies allowed the elucidation of DapL structures from the alga *C. reinhardtii* and the bacteria *C. trachomatis* [4-6].

This chapter describes the first X-ray crystal structure of *Vs*DapL.

5.2 Crystallisation and refinement.

Previously reported methods used to crystallise DapL, were trialed for the crystallisation of *Vs*DapL using the hanging drop-vapor diffusion method [4-6]. Over 3000 conditions were trialed, but after crystals failed to form subsequent changes of crystallisation conditions were made including the variation of buffers, pH range, salt concentrations, temperature, enzyme concentration and binding partners. Crystals of his-tagged *Vs*DapL appeared in a condition (60 % v/v T-mate pH 7.0) after 2 months containing two inhibitors, malic acid and maleic acid (Figure 5.1). The crystals were delicate square sheets measuring 100 μm in their largest dimension. Crystals were harvested and soaked in cryo-protectant solution and flash-frozen in liquid nitrogen (chapter 6, section 6.8.4). Crystals obtained in this condition diffracted to 2.25 Å and crystallised into the space group $P2_1$ with 2 chains present in the asymmetric unit. Diffraction data sets were processed using molecular replacement using Phaser [7], with a single chain of *C. reinhardtii* DapL (PDB: 3QGU) as the search model with ligands

and water removed prior to use. Crystallography and refinement statistics are noted in (Table 5.1).

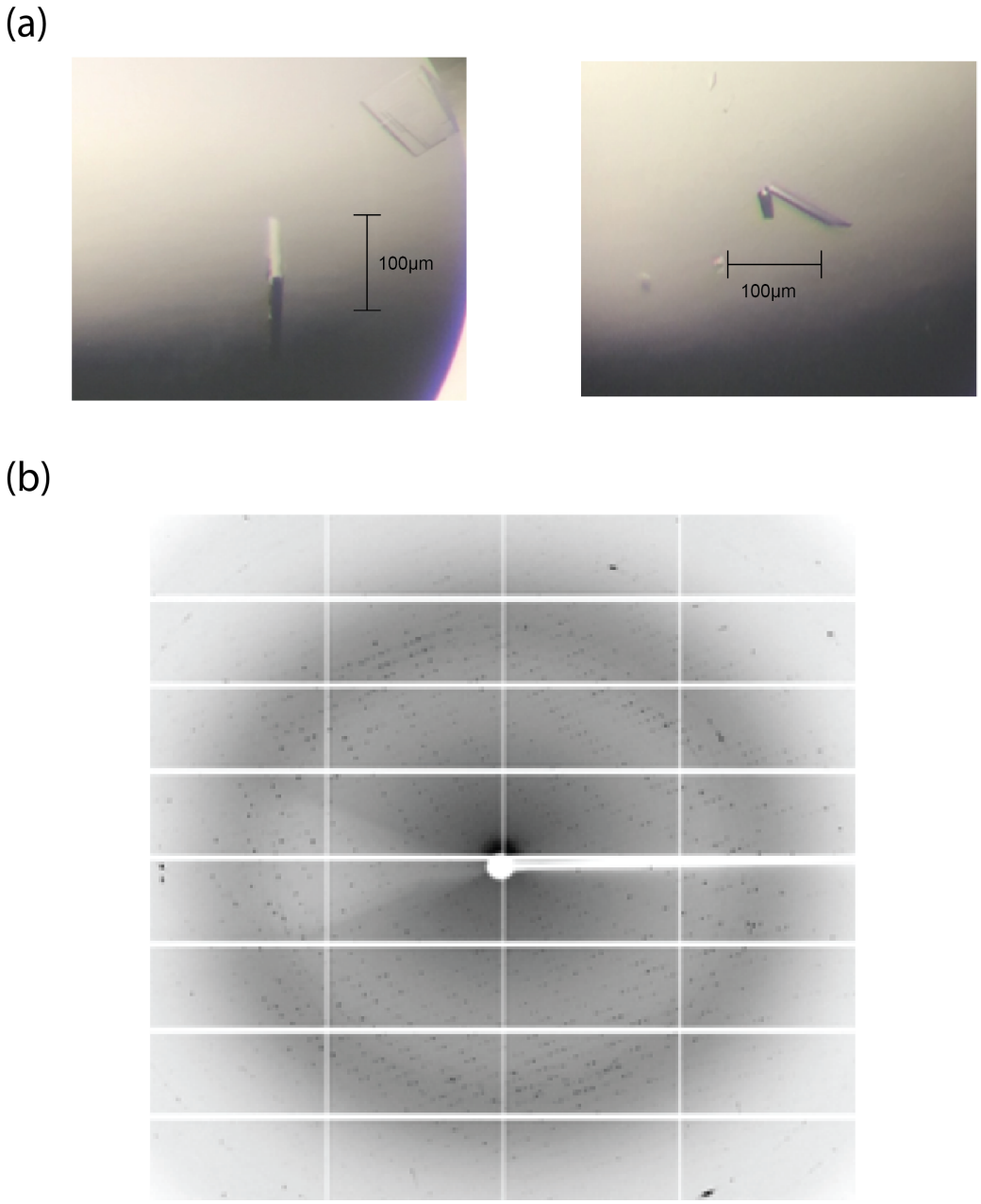

Figure 5.1: Protein Crystals of *Vs*DapL. (a) Crystals of *Vs*DapL that formed in the presence of maleic acid (left) and malic acid (right). (b) The diffraction scattering pattern of the crystal that diffracted to 2.25 Å.

Table 5.1: Data collection and refinement statistics

Data-collection statistics	*Vs*DapL
Diffraction source	Synchrotron
Wavelength (Å)	0.95366
Temperature (K)	110
Detector	Eiger 16 M
Number of images	200
Degrees	200
Space group	P 2_1
Cell dimensions:	
a, *b*, *c* (Å)	56.05, 121.37, 76.54
α,β, γ	90.00, 102.01, 90.00
Mol/asym. unit	2
Mosaicity (°)	0.14
Resolution (Å)	2.25 (2.33-2.25)
Unique reflections	179,143 (46,773)
$CC_{1/2}$	0.991 (0.577)
CC^*	0.998
R_{merge}	0.1081 (0.7179)
R_{-meas}	0.1262 (0.8384)
$I / \sigma I$	7.0 (1.3)
Wilson B-factor	31.94
Completeness (%)	99.1 (96.0)
Multiplicity	3.8
Refinement	
Resolution (Å)	2.25
No. reflections	179,143
Reflections used in refinement	46720 (4525)
Reflections used for R-free	2319 (214)
R-work	0.2029 (0.2908)
R-Free	0.2417 (0.3066)
CC (work)	0.946 (0.712)
CC (free)	0.901 (0.739)
Number of non-hydrogen atoms	6467
Macromolecules	6206
Ligand	50
Protein Residues	808
R.M.S deviations	
R.M.S Bonds (Å)	0.014
R.M.S Angles (°)	1.74
***Average B*-factors (Å^2)**	
Macromolecules	37.33
Ligands	92.07
Solvent	32.89
Ramachandran plot	
Ramachandran favoured (%)	95
Ramachandran allowed (%)	4.8
Ramachandran outliers	0.5
Rotamer outliers (%)	3.1
Clashscore	3.25

The final model contains 808/822 fitted amino acids and includes residues 1-68, 76-411 in both A and B chains. Poor electron density was observed for residues between R68 and P76 of both monomer chains, a region shown to comprise a flexible mobile loop region in other structures. Electron density was also poor for residues between S250 and V258 on both chains. Residues in this region were found to be highly conserved and form the contacts for the dimer interface and also the active site pocket.

5.3 General features of the *Vs*DapL crystal structure

The native *Vs*DapL monomer contains 411, amino acids but is likely to form a dimer of 822 amino acids at higher concentrations (Chapter 4). The solved crystalline structure is in agreement with the findings in chapter 4 of a dimeric oligomeric state and resembles a similar overall fold to previously reported DapL structures (Figure 5.2).

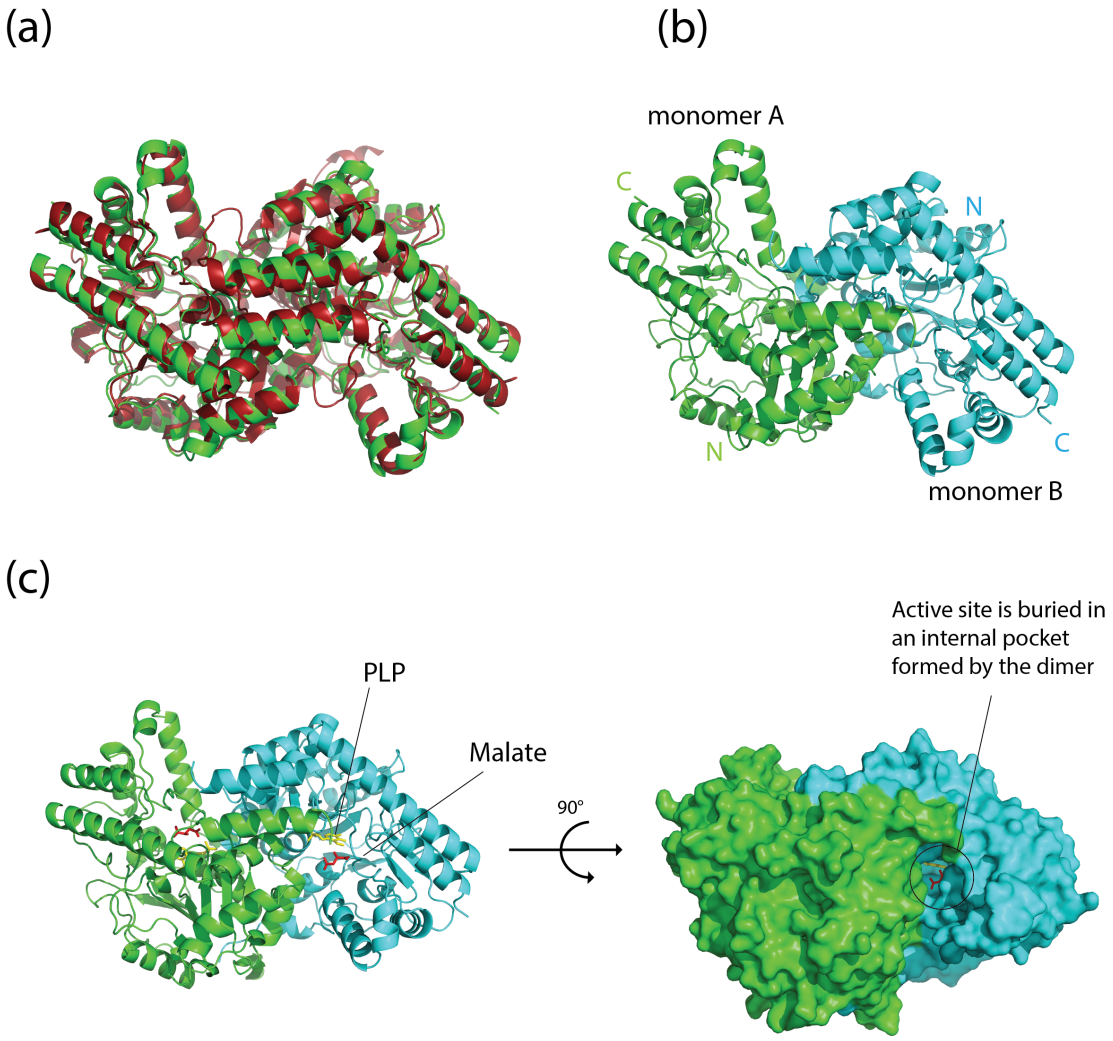

Figure 5.2: The solved crystal structure of *Vs*DapL shown in Pymol [8]. (a) The structure of *Vs*DapL (green) overlaid with the dimeric structure of *Cr*DapL (Red). (b) The homo-dimeric structure of *Vs*DapL indicating both monomers. N- and C- termini are labeled in the corresponding colours. (c) The structure of *Vs*DapL shown with the malate ion (red) bound in both active sites. The dimer is displayed in a surface space-filling model and is rotated 90° to outline one of the active sites binding pocket.

Secondary structure analysis revealed that the protein backbone contains both α-helices and β-sheets (chapter 4, section 4.2). This finding is supported this by the α/β type protein fold displayed in the crystal structure, however consistent with other reported structures, the backbone contains a higher content of α-helices. The overall protein fold of *Vs*DapL resembles type I aminotransferases, and reaffirms the suggestion that structure is conserved within PLP-dependent enzymes [9].

5.4 *Vs*DapL monomer features

Two chaliced-shaped monomers (A, B) are present in the asymmetric unit and are related by a non-crystallographic 2-fold axis and associate to form a homodimer, a typical feature of type I PLP-dependent aminotransferases [5]. Each monomer is comprised of a N-terminus arm (residues M1-L50), a large domain (LD) (residues P51-G325) and a small domain (SD) (residues N366-K411) and fold together to form a α-β-α complex (Figure 5.3).

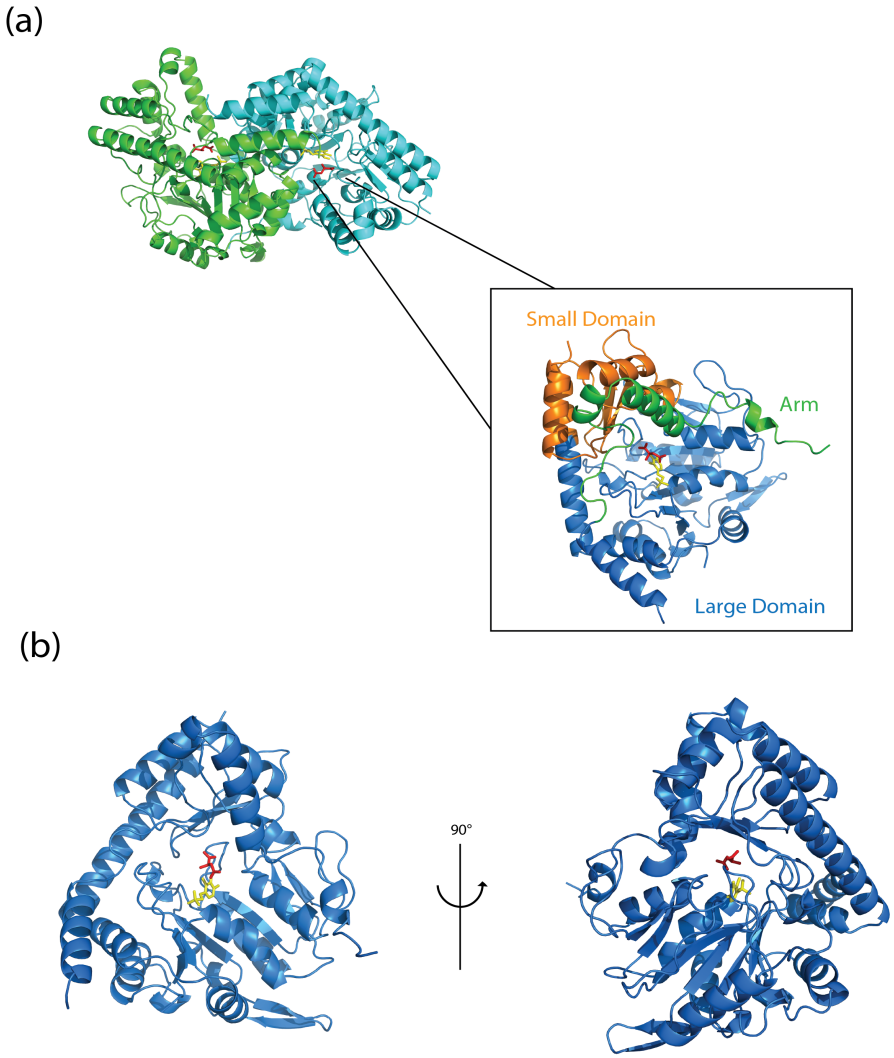

Figure 5.3: The *Vs*DapL monomer structure. (a) The three domains (LD, SD and arm regions) of the monomer and active site of *Vs*DapL with the malate ion (red) and PLP (yellow) bound. (b) The 90° rotation of the monomeric active of *Vs*DapL with the malate ion (red) and PLP (yellow) bound in the active site.

Protein sequence alignments and structural modeling of known DapL orthologues display that catalytic residues that comprise the active site stem from both monomers and are highly conserved, indicating that a dimeric oligomeric state is required for activity.

5.5 Dimer interface analysis

In solution, monomers A and B self-associate to form a homodimer. The dimeric interface contains two active sites located in an internal cavity of each monomer, consistent with the previously reported structures (Figure 5.4). PISA analysis of the *Vs*DapL structure shows that it has a weak dimer interface consisting of 83 residues (20.5%) from monomer A and 81 residues (20.0%) from monomer B [10]. Approximately 20% of the protein is solvent inaccessible as it is concealed in the interface, primarily held together with hydrogen bonds. Forming a homo-dimer from monomer A and B is enthalpically favorable as solvation gain is 14.5 kcal/mol, yet in solution the monomer and dimer associate very weakly with a $K_{d\ of}$ between 0.3 and 0.9 mg/mL (Chapter 4).

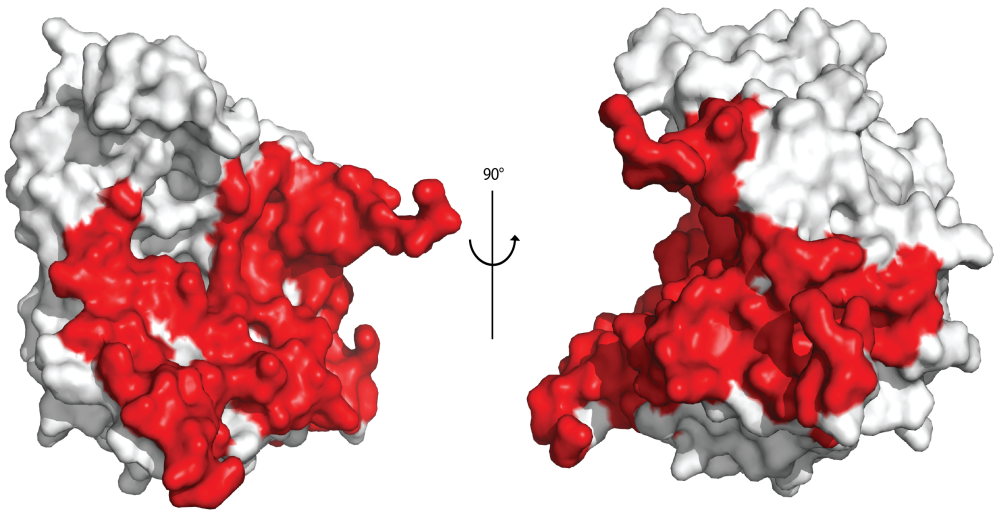

Figure 5.4: A surface model of the *Vs*DapL monomer displaying the residues in red that form the dimer interface.

A multiple sequence alignment of DapL orthologues shows that the residues that form that the dimeric interface in *Vs*DapL are not fully conserved in other orthologues. The discrepancy of conservation in these residues between organisms may explain the weak dimer interface that is seen in *Vs*DapL.

Figure 5.5: A multiple sequence alignment of VsDapL with the previously reported DapL orthologues. Red characters denote the residues involved in the dimeric interface. Green–highlighted areas denote motifs that are involved in active site formation. Blue-highlighted residues are the residues found to be involved in active site contacts. Symbols below the sequence alignment relate to the conservation between sequences, where * is fully conserved.

5.6 *Vs*DapL active site architecture

Homology modeling and sequence alignment reveal that there are 10 highly conserved residues involved in substrate binding (Figure 5.5). In the *Vs*DapL structure, 9/10 active site residues have been fitted. They are, I43, G44, K111 Y134, N189, K251 and R390 from one monomer and Y74*, E77* and N294* from the opposing monomer (Figure 5.6). As noted previously, the density for the residues between R68 and P76 on both chains was poor and therefore the residue Y74* could not be resolved in the *Vs*DapL structure. However a position in the active site is available where the Y74* residue has been reported to be found (Figure 5.6).

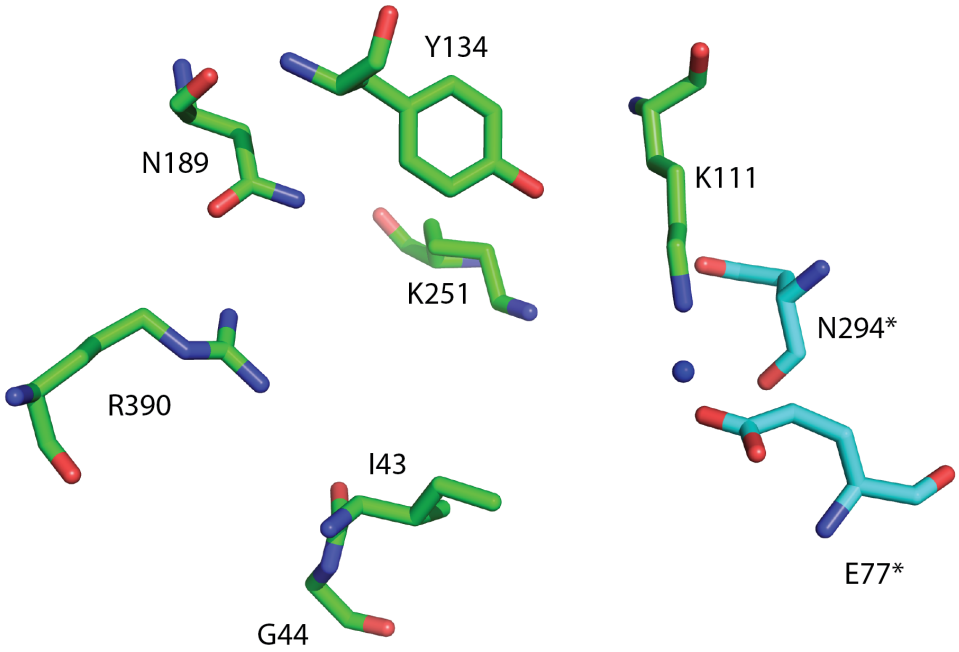

Figure 5.6: The active site architecture of *Vs*DapL. Residues from the opposing monomer are coloured in blue and are signified with the * sign. A gap exists (shown in the bottom right of the figure) where Y74* is shown to be located in other DapL orthologues.

5.6.1 Malate Binding site

*Vs*DapL was crystallised in the presence of two previously identified inhibitors, malic acid (200mM) and maleic acid (100 mM) [6]. At pH 7.6, both inhibitors form their corresponding ions, malate and maleate (Figure 5.7).

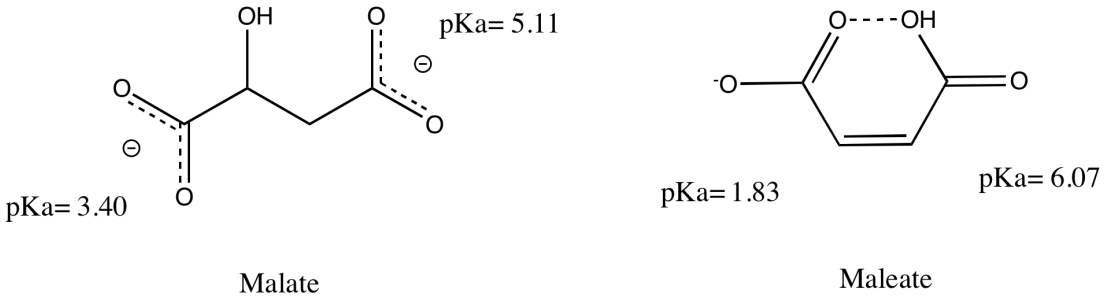

Figure 5.7: The chemical structures of the malate and maleate ions. Adapted in CHEMDRAW [6].

Electron density in the position where the malate/maleate ion has been reported to bind was reported in the *Vs*DapL (Figure 5.8). The density more closely resembled the malate ion, over the maleate ion and therefore the malate ion was modeled into the crystal structure. The malate ion is shown to form interactions with nearby active site residues and is consistent with previously reported structures. A nearby water molecule located in the active site, has been shown to form an interaction with the malate ion in previous structures. However in the *Vs*DapL structure, the water molecule does not form a contact with the malate ion suggesting that the malate ion may not be in the right orientation (Figure 5.8).

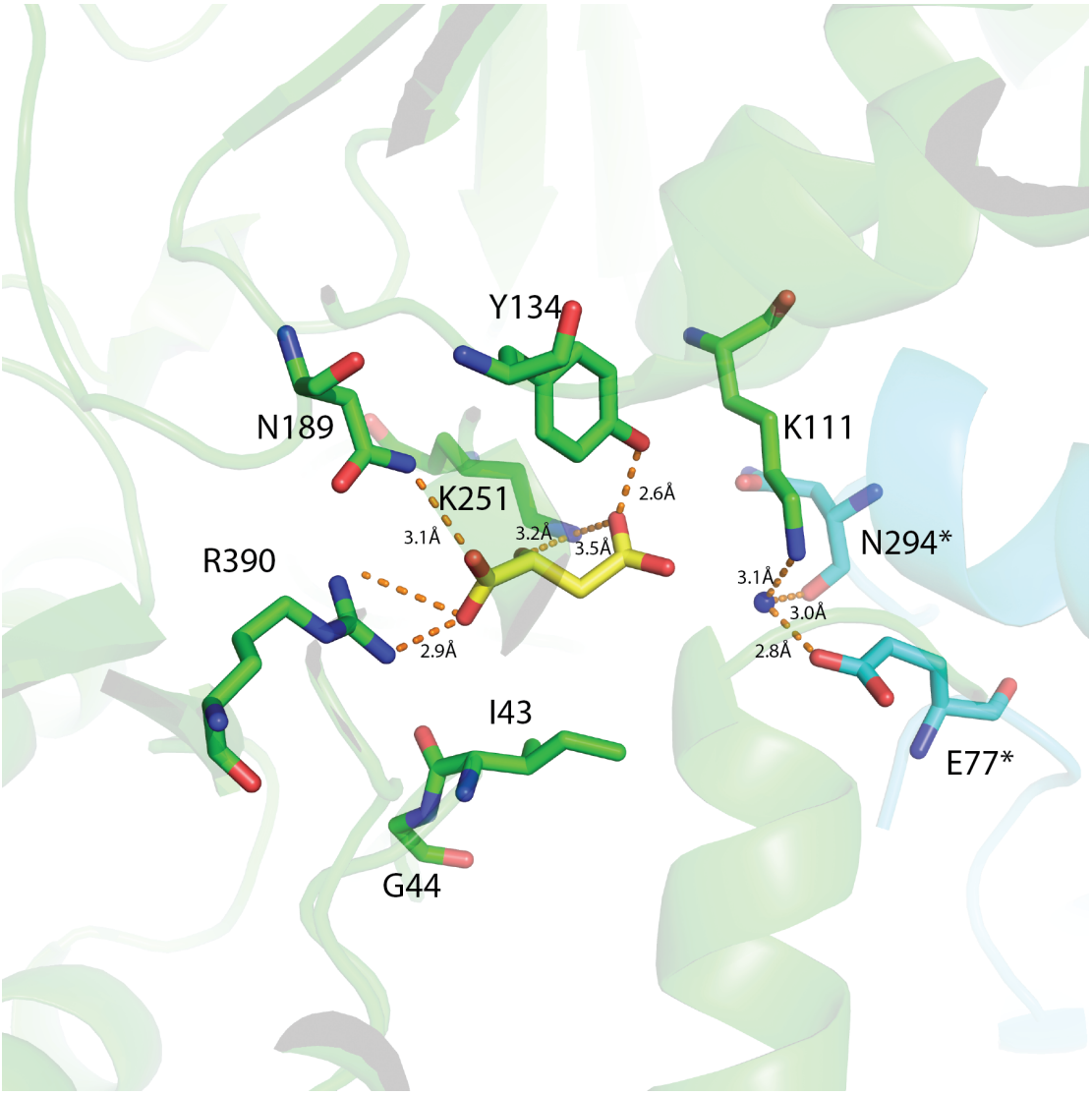

Figure 5.8: The malate binding site of *Vs*DapL. Malate is shown in yellow**,** residues from monomer A are shown in green and residues from monomer B are shown in blue. Residues are coloured by element and interactions are shown using orange dashed lines.

5.6.2 PLP Binding site

Located in close proximately to the malate ion in the active site, is the co-factor pyridoxal-5-phosphate. PLP is an essential part of the transaminase reaction and is covalently bound to the active site residue K251 through an imine linkage [11]. The electron density for PLP in active site in *Vs*DapL is in line with previous structural studies that have reported the position of PLP. PLP has been shown to form bonds with several active site residues including the favourable pi-pi stacking with Y134 (Figure 5.8).

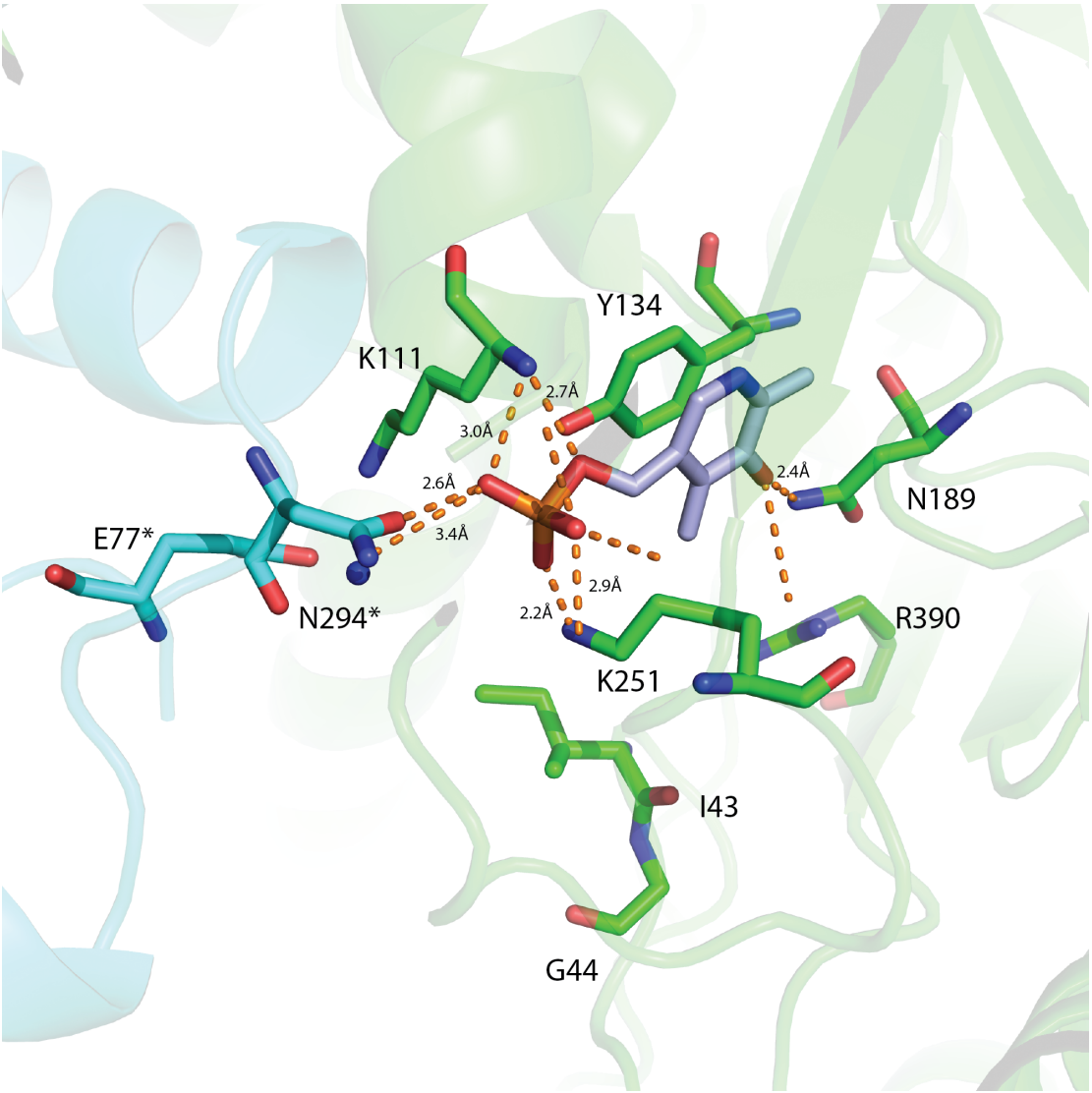

Figure 5.9: The PLP binding site of *Vs*DapL. PLP is shown in grey**,** residues from monomer A are shown in green and residues from monomer B are shown in blue. Residues are coloured by element and interactions are shown using orange dashed lines.

However, when PLP is modeled in the *Vs*DapL crystal structure with the malate ion present, the suggested position for forms fewer contacts with the conserved residues in the active site than in previously reported structures (Figure 5.10). The density for the PLP and the binding residues is ill defined, perhaps suggesting that this region is more dynamic or that PLP has multiple binding conformations.

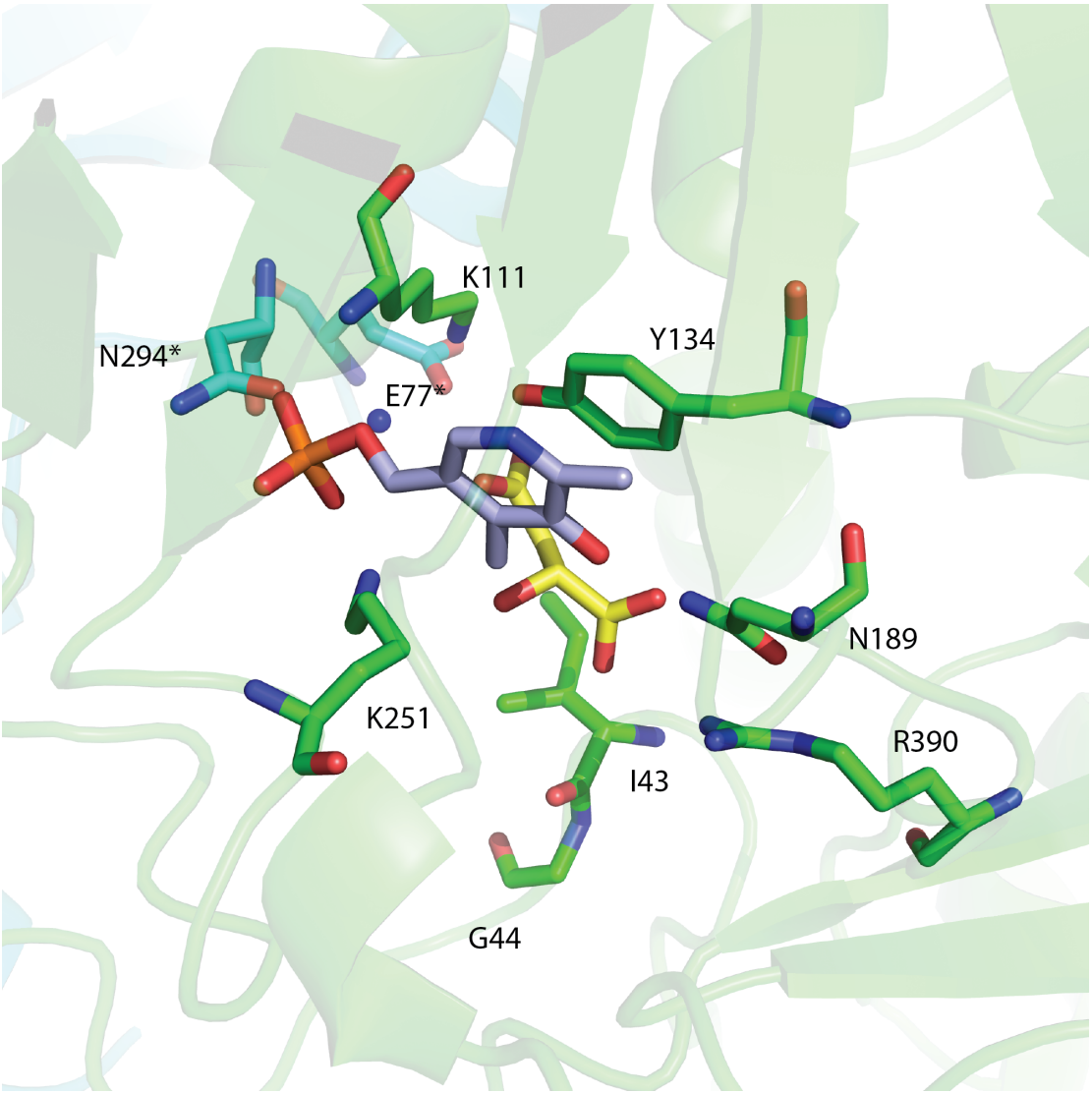

Figure 5.9: The PLP binding site of *Vs*DapL with the malate ion present. PLP is shown in grey, residues from monomer A are shown in green and residues from monomer B are shown in blue. Residues are coloured by element and interactions are shown using orange dashed lines.

5.7 Summary

In this chapter, the first X-ray crystal structure of *Vs*DapL was solved. This was done by co-crystallisation of *Vs*DapL with the inhibitor malic acid/maleic acid. The crystals diffracted to 2.25 Å and the structure was solved using molecular replacement. Above 95% of the residues were fitted to the electron density, however a region between R68 and P76 could not be solved. An ill-defined region between serine S250 and V258 that forms that active site binding pocket was fitted. The overall crystalline structure of *Vs*DapL was reported to adopt a dimeric state consistent with what was found for

the enzyme in solution in chapter 4. The dimer is comprised of two monomers (A, B) and are related by a non-crystallographic 2-fold axis consistent with type I aminotransferases. A multiple sequence alignment shows that the dimeric interface residues are not highly conserved while active site residues are highly conserved between organisms The active site density reported for the co-crystallised substrates were in line with previously reported structures and were modeled into the *Vs*DapL structure.

5.8 References

[1] Smyth, M. S., and Martin, J. H. (2000) x ray crystallography, *Mol Pathol 53*, 8-14.

[2] Fraser, J. S., van den Bedem, H., Samelson, A. J., Lang, P. T., Holton, J. M., Echols, N., and Alber, T. (2011) Accessing protein conformational ensembles using room-temperature X-ray crystallography, *Proc Natl Acad Sci U S A 108*, 16247-16252.

[3] Flack, H. D., and Bernardinelli, G. (2008) The use of X-ray crystallography to determine absolute configuration, *Chirality 20*, 681-690.

[4] Dobson, R. C., Giron, I., and Hudson, A. O. (2011) L,L-diaminopimelate aminotransferase from *Chlamydomonas reinhardtii*: a target for algaecide development, *PLoS One 6*, e20439.

[5] Watanabe, N., Clay, M. D., van Belkum, M. J., Fan, C., Vederas, J. C., and James, M. N. (2011) The structure of LL-diaminopimelate aminotransferase from *Chlamydia trachomatis*: implications for its broad substrate specificity, *J Mol Biol 411*, 649-660.

[6] Watanabe, N., Cherney, M. M., van Belkum, M. J., Marcus, S. L., Flegel, M. D., Clay, M. D., Deyholos, M. K., Vederas, J. C., and James, M. N. (2007) Crystal structure of LL-diaminopimelate aminotransferase from *Arabidopsis thaliana*: a recently discovered enzyme in the biosynthesis of L-lysine by plants and Chlamydia, *J Mol Biol 371*, 685-702.

[7] McCoy, A. J., Grosse-Kunstleve, R. W., Adams, P. D., Winn, M. D., Storoni, L. C., and Read, R. J. (2007) Phaser crystallographic software, *Journal of Applied Crystallography 40*, 658-674.

[8] L DeLano, W. (2002) *The PyMOL Molecular Graphics System (2002) DeLano Scientific, Palo Alto, CA, USA*. http://www.pymol.org.

[9] McKinnie, S. M., Rodriguez-Lopez, E. M., Vederas, J. C., Crowther, J. M., Suzuki, H., Dobson, R. C., Leustek, T., Triassi, A. J., Wheatley, M. S., and Hudson, A. O. (2014) Differential response of orthologous L,L-diaminopimelate aminotransferases (DapL) to enzyme inhibitory antibiotic lead compounds, *Bioorg Med Chem 22*, 523-530.

[10] Krissinel, E., and Henrick, K. (2007) Inference of macromolecular assemblies from crystalline state, *J Mol Biol 372*, 774-797.

[11] Alexander, F. W., Sandmeier, E., Mehta, P. K., and Christen, P. (1994) Evolutionary relationships among pyridoxal-5′-phosphate-dependent enzymes, *European Journal of Biochemistry 219*, 953-960.

Discussion

The biosynthesis of L-lysine through the diaminopimelate pathway is an appealing target for the development of algaecides, herbicides and therapeutics, as the pathway is absent in animals but present in bacteria, plants and algae. One of the pathways within the Dap pathway catalysed by the enzyme diaminopimelate aminotransferase (DapL) had been characterised in three previous organisms, *Arabidopsis thaliana*, *Chlamydomonas reinhardtii* and *Chlamydia trachomatis,* however each organism can synthesise L-lysine through alternative routes. The bacterium *Verrucomicrobium spinosum* on the other hand, only synthesises L-lysine using DapL and as such was used as a model organism for the viability of this enzyme as a target. Presented for the first time in this thesis is the kinetic, biophysical and structural characterisation of DapL *V. spinosum.*

When elucidating the kinetic parameters of *Vs*DapL, it was found that the enzyme is quite inefficient in respect to its substrate, L,L-Dap. The biophysical and structural studies may offer an explanation into why this is. Our biophysical studies show that in solution at concentrations at and below 0.3 mg/mL, *Vs*DapL exists in a primarily monomeric state. However as the concentration increases, the proportion of monomeric species to dimeric species increases, demonstrating a monomer-dimer equilibrium. Previous studies structural for DapL show it to exist in a dimeric state with residues comprising the active site to come from both monomers, indicating that a dimeric oligomeric state is required for activity. This was consistent with what was found in the solved crystal structure for *Vs*DapL as it resembled a typical type I aminotransferase enzyme. As the attempted assays were at a low concentration of enzyme, it is likely that the species in solution was monomeric and thus full activity is not seen and resulted in the kinetic parameters given. The structural analysis of *Vs*DapL also shows that residues that comprise the dimeric interface are not conserved between organisms and may contribute to why this monomer-dimer equilibrium is seen in *Vs*DapL and is not in other organisms that use DapL. The monomer dimer-equilibrium may be a result of *V. spinosum* exclusively using the DapL pathway for L-lysine biosynthesis, however further studies are required to assess whether this is a true feature.

To summarise, presented in this work is the first kinetic, biophysical and structural characterisation of the enzyme diaminopimelate aminotransferase (DapL) from ta novel organism which solely uses DapL for L-lysine biosynthesis.

Chapter Six - Methods and Materials

6.1 Chemicals, materials and general equipment

Unless stated otherwise, general reagents and chemicals that were purchased through Sigma-Aldrich, Applichem, Molecular dimensions and Hampton Research.

All Eppendorf tubes and pipette tips were sterilised by autoclaving (121°C for 20 minutes).

All protein and DNA experimental work was conducted on ice or at 4°C. DNA and protein solutions were temporarily stored at 4°C unless otherwise stated.

6.2 Stock solutions

All buffers, reagents and solutions requiring H_2O were prepared with Milli-Q H_2O, and filtered with a 0.22 μm filter.

Stock solutions of isopropyl β-d-1-thiogalactopyranoside (IPTG) were prepared with Milli-Q H_2O, filtered with a 0.22 μm filter and stored at -20°C in aliquots.

All prepared antibiotics were filtered with a 0.22 μm filter and stored at -20°C (Table 6.1).

Table 6.1: Antibiotic concentrations

Antibiotic	Prepared concentration (mg/mL)	Working concentration (μg/mL)
Kanamycin	30	30
Chloramphenicol	30	30
Ampicillin	100	100

6.3 Molecular biology

6.3.1 Bacterial work and strains

All work with bacteria was completed using aseptic techniques, inside either a laminar flow cabinet or beside a flame. All equipment was sterilised by autoclaving.

The pET-30a (+) plasmid (kanamycin resistance) encoding the gene for his-tagged *Verrucomicrobium spinosum* diaminopimelate aminotransferase (DapL) was generously supplied by the co-supervisor of this work, Associate Professor André O. Hudson of The Rochester Institute of Technology.

6.3.2 Protein sequence

Protein sequence of DapL from *Verrucomicrobium spinosum* (411 amino acids) obtained from the NCBI website.

1 MALINENFLK LKAGYLFPEI ARRVKAFTEG NPEAAQRLIR CGIGDVTEAL PEAVRYAMHE
61 AVDELGNRST FKGYGPEQGY DFLRNAIADN DYKARGLPIE ADEIFISDGS KCDTGNILDI
121 FGQGNTIAIT DPVYPVYVDT NVMIGNTGEA DENGAYAGLV YLKCTPENGF VPDIPQEKAD
181 LIYLCYPNNP TGAVATRPQL EAWVKYAREN GSVLLYDAAY EAFIQDPTIP HSIFEIEGAR
241 DCAIEFRSFS KNGGFTGVRC AYVVIPKSLM GRKKNGEAQA LHPLWSRRHS TKFNGASYIV
301 QKGAEALYTD EGKSQTKALI EHYMGNAALL VEACKNAGLS VFGGVNAPYV WVGCPAGLTS
361 WQMFDKMLNE ANVVITPGSG FGSAGEGYFR ISAFNSRANV EEVCRRIAAL K

6.3.3 Media

Luria-Bertani (LB) medium was prepared using 25 g of powder per 1 L of Milli-Q H_2O and was autoclaved at 121°C for 20 minutes.

6.3.4 Agar plates

LB agar was prepared using a 5:3 ratio of LB powder to agar e.g. 25 g LB powder: 15 g of agar per 1 L. Following autoclaving and cooling to 50°C, an appropriate antibiotic was added as a 1000x stock (section 6.2). Approximately 25 mL was then poured into each petri dish and left to solidify for 30 minutes in a laminar flow cabinet.

6.3.5 Starter culture preparation

Agar plates containing the appropriate antibiotic were streaked using a sterilised spreader or pipette tip with a glycerol stock (section 6.3.6). Positive and negative controls were prepared by streaking with chloramphenicol, ampicillin or no antibiotic.

The plates were then incubated at 37°C overnight (14-16 hours). A colony was then picked using a sterile pipette tip and used to inoculate fresh LB media (5-200 mL) containing the appropriate antibiotic. The media was then incubated at 190 rpm and 37°C overnight (14-16 hours).

6.3.6 Glycerol stocks

Glycerol stocks were set up by mixing 500 µL of the overnight starter culture with 500 µL of 50% glycerol in 1.7 mL Eppendorf tube. The contents were mixed, snap frozen in liquid nitrogen and stored at -80°C.

6.3.7 Competent cell transformation

Competent BL21(DE3)* *Escherichia. coli* cells were thawed on ice and added to a cold Eppendorf tube containing 2-3 μL (80-100 ng) of plasmid containing *Vs*DapL. After mixing, the Eppendorf tube was incubated on ice for 30 minutes before being heat shocked in a heating block or water bath at 42°C for 60 seconds. Following the heat shock, the tube was placed adding 950 μL of Super Optimal Broth with catabolite repression (SOC) medium. The tube was then incubated at 37°C and 190 rpm for 60 minutes. Following this, 100 μL of the solution was plated onto a kanamycin agar plate. Contamination was checked by plating 100 μL of culture onto three control agar plates. These plates were as follows: a positive control plate with no antibiotics, and two negative control plates containing chloramphenicol and ampicillin. All agar plates were incubated at 37°C overnight (14-16 hours).

6.4 Protein Biochemistry

The methods and protocols within this section were performed using aseptic technique when appropriate and all protein work was completed either at 4°C or on ice.

6.4.1 Expression trials

Expression trials for *Vs*DapL were conducted using small-scale cultures of LB to find optimum expression condition. Glycerol stocks were streaked onto agar plates containing appropriate antibiotics. A single colony was picked using a sterilised pipette tip and added to 5-20 mL of LB with kanamycin. This culture was incubated overnight at 190 rpm and 37°C. Larger autoclaved cultures (20-100mL) containing kanamycin were inoculated using 5 mL of the overnight culture and incubated at 190 rpm and 37°C to an optical density at 600 nm (OD_{600}) of 0.4-0.6. Protein expression was then induced by adding 1 M IPTG to a final concentration of 1 mM. The culture was incubated overnight at 190 rpm and 26°C.

6.4.2 Testing for overexpression

Samples at different stages during the induction were taken for overexpression testing. Samples were taken at pre-induction, 2 hours; 6 hours and 14 hours post induction. Samples were analysed by SDS-PAGE for over-expression of *Vs*DapL (Section 6.4.4).

6.4.3 Full scale protein expression

Protein expression followed the same protocol as described in section 7.4.1 with slight modifications. Overnight cultures were used to inoculate 1 L cultures that were induced with 1 M IPTG to a final concentration of 1 mM. Following overnight induction, the cells were harvested by centrifugation at 8,000 x g for 15 minutes at 4°C. The supernatant was discarded and cell pellets were either put on ice for immediate purification or transferred into 50 mL falcons tubes and stored at -20°C.

6.4.4 Sodium dodecyl sulfate polyacrylamide gel electrophoresis

Sodium dodecyl sulfate polyacrylamide gel electrophoresis (SDS-PAGE) was used to visualise the purity of protein. Bolt® Pre-cast 4-12% Bis-Tris Plus 10 well or 15 well electrophoresis gels were supplied by Novex (Novex® by Life Technologies™). MES SDS 1x stock was used as the running solution for electrophoresis. Novex® Protein size estimation in kilo Daltons (kDa) was determined by loading 7 µL of Sharp Pre-Stained Protein Standard (Novex® by Life Technologies™) into one of the wells of the gel. Each used well contained 10 µL of protein sample, 16 µL of filtered Milli-Q H_2O, 10 µL of Bolt™ LDS Sample buffer 4x and 10 µL of reducing agent (Dithiothreitol (DTT) or Tris (2carboxyethyl) phosphine (TCEP) 10 mM). Samples were then heated to 80°C in a heating block for 10 minutes before loading 10 µL into appropriate wells of the gel (Table 6.2).

The gels were run at 165 V for 35 minutes and stained for 30 minutes using Coomassie brilliant blue stain. Coomassie blue was prepared by adding 1 g Coomassie dye to 450 mL methanol, 450 mL Milli-Q H_2O and 100 mL acetic acid.

Gels were destained using Coomassie destain (450 mL methanol, 450 mL water, 100 mL acetic acid) until the gel was de-stained sufficiently. Gels photos were imaged using a bio 5000 + microter scanner.

Table 6.2: SDS-PAGE sample components

Reagents	Reason	Volume (µL)
Milli-Q H_2O	To make up volume	16
DTT or TCEP	Reducing Agent	4
LDS	Dye/stain	10
Protein Sample	Sample	10
Total		**40**

6.4.5 Cell lysis

Cell pellets were thawed on ice and fully re-suspended in 20-30 mL IMAC binding buffer 1 (Table 6.3), then lysed by sonication for 12 minutes at 70% frequency and 0.5 second interval. Following lysis, the solution was centrifuged at 13,000 x g at 4°C for 15 minutes. The supernatant (crude lysate) was carefully collected, transferred to a sterile 50 mL Falcon tube and kept on ice.

Table 6.3: Expression and purification buffers.

Buffers	Buffer Solution
IMAC Buffer 1 Non-Specific Binding	50 mM sodium phosphate, 300 mM NaCl, 40 mM Imidazole, pH 8.0.
IMAC Buffer 2 Elution Buffer	50 mM Sodium Phosphate, 300 mM NaCl, 250 mM Imidazole, pH 8.0.
Dialysis Buffer	50 mM Sodium Phosphate, 300 mM NaCl, 40 mM Imidazole, 0.3 mg/mL Enterokinase pH 8.0.
Size Exclusion buffer 1 (SEC)	20 mM Tris, 150 mM NaCl, pH 7.6.
Size Exclusion buffer 2 (SEC)	100 mM HEPES-KOH, 1 mM DTT, 2 mM EDTA, pH 7.6.
Size Exclusion buffer 3 (SEC)	20 mM HEPES-KOH, 100 mM NaCl, 1 mM DTT, pH 7.6.

6.5 Protein purification

6.5.1 Immobilised metal affinity chromatography (IMAC)

Immobilised metal affinity chromatography (IMAC) was used as the first purification step. The 5 mL IMAC column (GE healthcare) was first equilibrated by running through 25 mL of Milli-Q H_2O followed by 15 mL of IMAC buffer 2 containing high imidazole to prime the column. As the final equilibration step, 15 mL of IMAC buffer 1 containing low imidazole was run through the. The crude lysate was then loaded onto the column and washed with 25 mL of IMAC buffer 1. The flow through was collected and run back through the column to ensure maximum binding of protein to the column. The protein was then eluted with 10 mL of IMAC buffer 2 containing high imidazole and collected in 0.5 mL fractions. These fractions were tested using SDS-PAGE (section 6.4.4) and fractions containing protein of interest were pooled. A sample was taken to estimate protein concentration using the A_{280} Nanodrop or the Bradford assay (section 6.5.4)

6.5.2 His-tag cleavage

A semi permeable dialysis membrane was knotted at one end and loaded with a 2mL of his-tagged *Vs*DapL. The other end was then tied and both ends were clipped before being submerged in 2 L of dialysis buffer containing enterokinase (Table 6.3). This was then placed on a magnetic stirrer at 4°C and left to equilibrate for 24 hours. After 24 hours the tubing was cut open and the protein solution was carefully removed. This solution was loaded onto the his-Trap column, washed with 5 mL IMAC buffer 1 (Table 6.3) and the flow through was collected.

6.5.3 Buffer exchange

Pooled fractions containing *Vs*DapL were added to a 30 kDa MWCO spin concentrator (Sartorius), and concentrated down to 2 mL by centrifugation at 7000 rpm and 4°C in 10 minute intervals. Between each interval the protein was mixed

using a pipette to prevent aggregation. The spin concentrator was refilled a minimum of three times to 20 mL using the desired buffer and centrifuged down to a final volume of 1.5 mL.

6.5.4 Size exclusion column chromatography (SEC)

Size exclusion chromatography (SEC) was used in the two-step purification of *Vs*DapL to separate proteins that may have co-eluted with *Vs*DapL during IMAC purification. A pre-packed 120 mL Superdex 200 gel filtration column (GE Healthcare was equilibrated with 500 mL of desired SEC buffer (Table 6.3). *Vs*DapL was concentrated to 1.5 mL injected onto the column and run with 120 mL of equilibrated buffer at 0.3 mL per minute. Fractions were collected in a 96 well plates and analysed by SDS-PAGE. Following SDS-PAGE fractions containing pure *Vs*DapL were pooled and concentrated using a 30 kDa MWCO spin concentrator (Sartorius), before being aliquotted into different volumes, snap frozen in liquid nitrogen and stored at -80 °C

6.5.5 Protein concentration determination

Most protein concentration measurements were determined using a Nanodrop ND-1000 spectrophotometer at 280 nm. Protein concentration was calculated using the extinction coefficients at 280 nm (52300, 1.69 g/L), calculated from the amino acid sequence using exPASy ProtParam and beer's law [1]. The Bradford assay was also used as another method for determining the concentration of protein samples [2]. The spectrophotometer was blanked using 800 µL Milli-Q H_2O and 200 µL Bio-Rad Dye. Samples were mixed and left for at least 5 minutes at room temperature before being read at 595 nm. Protein concentrations were calculated using a calibration curve from bovine serum albumin (BSA).

Table 6.4: Components of the Bradford assay

Reagents	Volume (µL)
Protein Sample	80
Milli-Q H_2O	720
Bio-Rad Dye	200
Total	**1000**

6.6 Kinetics

All kinetics measurements were performed in triplicate. Buffer and reagent solutions used in the assays were filtered using a 0.22 µm filter when appropriate and either kept on ice or at 4°C. Serial dilutions were used to achieve desired concentrations of reagent and protein solutions. Protein concentration was confirmed using the Nanodrop A_{280}. Activity and inhibition of *Vs*DapL were measured using an adapted version of the *ortho*-aminobenzaldehyde assay [3, 4]. All assays were performed in triplicate at 30°C over 200 minutes.

6.6.1 The *o*-Aminobenzaldehyde assay

*Vs*DapL was thawed from 80°C on ice and centrifuged at 14,000 x g and 4°C for 15 minutes before use. Appropriate concentrations were then made up using serial dilutions in the desired buffer. All reagents (Table 6.5) were added to a 1.7 mL Eppendorf tube and incubated at 30°C for 15 minutes before being transferred into a 1 mL cuvette. The spectrophotometer was blanked against buffer during this incubation period. The cuvette was then placed in the spectrophotometer followed by the addition of 50 µL of buffer. As the last step for all assays, 100 µL of *Vs*DapL at the desired concentration for the assay was added, bringing the final volume to 1 mL. The contents of the cuvette were thoroughly mixed using a pipette and the absorbance was tracked at 440 nm over 200 minutes. Controls containing no substrate in the presence of *Vs*DapL, and substrate without *Vs*DapL, were also set up and measured simultaneously.

Table 6.5: The *o*-aminobenzaldehyde assay reagents

Reagents	Stock concentration	Working concentration	Volume (µL)
L,L-DAP	50 mM	2.3 mM	39.1
α-Ketoglutarate (2OG)	200 mM	10 mM	42.5
o-aminobenzaldehyde	100 mM	8.3 mM	70.55
Buffer-100 mM Hepes-KOH pH7.6	-	-	747.85
*Vs*DapL	2.87 mg/mL	0.5 mg/mL	100
Total			**1000**

6.6.2 The *o*-Aminobenzaldehyde inhibition assay

A stock solution (200mM) of the inhibitor, malic acid, was prepared in Milli-Q H_2O and adjusted to pH 7.0 with NaOH. The *o*-aminobenzaldehyde assay was then set up as per section 6.6.1 (Table 6.6). Desired concentrations of the inhibitor were added to the 1.7 mL eppendorf tubes to a final volume of 850 µL and incubated at 30°C for 15 minutes before being transferred into a 1 mL cuvette. The cuvette was then placed in the spectrophotometer followed by the addition of 50 uL of buffer. As the last step, 100 µL of *Vs*DapL at the desired concentration for the assay was added, bringing the final volume to 1 mL. An additional control was also set up containing substrate and enzyme but no inhibitor. The absorbance was monitored at 440 nm over 200 minutes.

Table 6.6: The *o*-aminobenzaldehyde assay reagents. Both the malic acid and buffer volumes changed depending on the amount of inhibitor that was required in the assay

Reagents	Stock concentration	Working concentration	Volume (µL)
L,L-DAP	50 mM	2.3 mM	39.1
α-Ketoglutarate (2OG)	200 mM	10 mM	42.5
o-aminobenzaldehyde	100 mM	8.3 mM	70.55
Malic acid	200 mM	-	-
Buffer-100 mM Hepes-KOH pH7.6	-	-	-
*Vs*DapL	2.87 mg/mL	0.5 mg/mL	100 µL
Total			**1000**

6.6.3 Kinetic data analysis

The data collected from the assays was analysed the GraphPad Prism 6 software. The kinetic parameters K_M and V_{max} were found by plotting the substrate concentration the maximum velocity at 440 nm. Inhibitor parameters including K_I were found by plotting the concentration of inhibitor against the maximum absorbance at various substrate concentrations at 440nm.

6.7 Biophysical Techniques

6.7.1 Far-UV circular dichroism spectroscopy

6.7.1.1 Buffers and sample preparation

Purified *Vs*DapL stored in 20 mM Tris-HCl, 150 mM NaCl at pH 7.6 was thawed on ice and centrifuged at 14,000 x g for 15 minutes at 4°C. It was then diluted to 1 mg/mL in the same buffer followed by a further dilution in Milli-Q H_2O to give a final concentration of 0.01 mg/mL. Then buffer was diluted by the same amount in dilution in Milli-Q H_2O for a reference blank.

6.7.1.2 Wavelength scans

The buffer blank was loaded into a Jasco J-815 circular dichroism (CD) spectrometer in a 2 mm path length quartz cuvette and a reading was taken. The cuvette was carefully cleaned and loaded with sample, and a far-UV spectra was taken between 190 and 260 nm at 20°C. The reported spectra were the average of three scans that were corrected for buffer blank.

6.7.1.3 Temperature/wavelength thermal melt scans

*Vs*DapL was diluted to 0.05 mg/mL as per section 6.7.1.1 and loaded into a 10 mm path length cuvette. The instrument was blanked with buffer then loaded with the sample and an initial scan was taken between 190-260 nm. Thermal denaturation was monitored by recording the ellipticity at 220 nm with data collected at 0.3 intervals between 25°C and 95°C. Three wavelength scans were also taken every 10°C and averaged.

6.7.2 Analytical ultracentrifugation

6.7.2.1 Sample preparation

Purified *Vs*DapL stored in 20 mM Tris-HCl, 150 mM NaCl at pH 7.6 was thawed on ice and centrifuged at 14,000 x g for 15 minutes at 4°C. Concentrations of of 0.3, 0.6 and 0.9 mg/mL were obtained by serial dilutions in the same buffer and confirmed by Nanodrop at A_{280}.

6.7.2.2 Sedimentation velocity

Analytical ultracentrifugation (AUC) sedimentation velocity experiments were performed at 30°C in a Beckman Coulter XL-I analytical ultracentrifuge using double sector quartz cells in an 8-hole AN-50 TI rotor. Data was obtained at 50,000 rpm using 380 µL of protein at 0.3, 0.6 and 0.9 mg/mL. Scans were taken at 280 nm and data was collected using absorbance optics.

6.7.2.3 Data Analysis

The program SEDNTERP was used to calculate buffer density and viscosity and an estimation of the partial specific volume of *Vs*DapL [5]. The program SEDFIT was used

to fit experimental data to a continuous sedimentation coefficient c(s) model [6]. The program, WinHydroPRO was used to estimate the sedimentation coefficient for the dimer of *Vs*DapL from the molecular model [7] .

6.7.3 Small angle X-ray scattering

Small angle X-ray scattering (SAXS) data for *Vs*DapL was collected on the SAXS/WAXS beamline equipped with a Pilatus 1 M detector (170 mm x 170 mm, effective pixel size 172 x172 μm) at the Australian Synchrotron. The wavelength of the X-rays was 1.0332 Å. The sample detector distance was 2400 mm, providing a *q* range of 0.01-0.3 $Å^{-1}$. *Vs*DapL at 10 mg/mL was injected onto an inline Superdex S200 5/150 Increase (GE Healthcare), equilibrated with 20 mM Tris-HCl, 150 mM NaCl at pH 7.6 and supplemented with the radical scavengers 5 % (v/v) glycerol and 0.1 % (w/v) sodium azide, using a flow rate of 0.45 mL/minute. Coflow SAXS was used to minimize sample dilution and maximise signal to noise. Scattering data was collected in 2-second exposures over the course of the elution using a 1.5 mm glass capillary at 285 K (12°C).

6.7.3.3 Data analysis

Data analysis was performed using the ATSAS 2.7 Package [8]. Guinier fits were performed using PRIMUS [9]. Indirect Fourier transforms to give P(r) was calculated using GNOM [10]. Theoretical SAXS scattering curves of the *Vs*DapL crystal structure was generated from atomic coordinates and compared with the experimentally determined scattering curves using SREFLEX [11].

6.8 X-ray crystallography

6.8.1 Initial crystallisation trials

Purified *Vs*DapL was concentrated to 10, 20 and 39 mg/mL in three different buffers (Table 6.3). Screening against possible crystallisation conditions in the three buffers was conducted using a range of screens (Molecular Dimensions Ltd) (Table 6.7). A multichannel pipette was used to transfer 35 µL of each condition from the screen into 96 well plates. The plates were loaded onto a TTP Labtech mosquito® crystal robot and 200 nL of protein was mixed via a robot with 200 nL of each condition giving a final volume of 400 nL in each drop. The 96 well plates were then stored at either 8°C or 20°C.

6.8.2 Co-crystallisation crystal trials

Co-crystallisation of *Vs*DapL was attempted following the protocol described in section 6.8.1, but prior to the mosquito crystal robot use the protein was mixed at a 1:1 ratio with one of three binding partners (malic acid 200 mM, maleic acid 200 mM and L,L Dap 20 mM). The plates were loaded onto the mosquito crystal robot and 200 nL of protein/inhibitor solution was mixed with 200 nL of each condition for a final volume of 400 nL in each drop. The 96 well plates were then stored at either 8 °C or 20 °C.

Table 6.7: Trailed crystallisation screens.

Crystal screens (Molecular Dimensions Ltd)	Crystal hits condition
SG1 Screen HT-96	Well G5 (with malic and maleic acid)
Structure Screen 1 + 2	-
LMB Crystallisation screen	-
Morpheus	-
Clear Strategy II	-
JCSG-Plus	-
PACT Premier	-

6.8.4 Experimental

Crystals were harvested with a litho-loop and soaked in a cryo protectant solution containing 85% of crystallisation solution (SG1 Screen HT-96, well G5) and 15% of a master solution (50% glycerol and 50 % ethylene glycol) before being flash-cooled in liquid nitrogen. Diffraction data was collected at 110K on the MX2 beamline at the Australian Synchrotron at a wavelength of 0.9537 Å.

6.8.5 Data analysis and structure determination

Diffraction images were indexed and integrated using iMOSFLM [12]. Scaling and data reduction was performed using SCALA from the CCP4 Program suite [13]. Molecular replacement was performed using MolRep using the crystal structure of CrDapL (PDB: 3QGU) as the search model [14]. The structure was refined using REFMAC [15] and PHENIX [16] . Model rebuilding was performed using Coot [17].

6.9 References

[1] Wilkins, M. R., Gasteiger, E., Bairoch, A., Sanchez, J. C., Williams, K. L., Appel, R. D., and Hochstrasser, D. F. (1999) Protein identification and analysis tools in the ExPASy server, *Methods Mol Biol 112*, 531-552.

[2] Bradford, M. M. (1976) A rapid and sensitive method for the quantitation of microgram quantities of protein utilizing the principle of protein-dye binding, *Anal Biochem 72*, 248-254.

[3] Hudson, A. O., Singh, B. K., Leustek, T., and Gilvarg, C. (2006) An LL-diaminopimelate aminotransferase defines a novel variant of the lysine biosynthesis pathway in plants, *Plant Physiol 140*, 292-301.

[4] McKinnie, S. M., Rodriguez-Lopez, E. M., Vederas, J. C., Crowther, J. M., Suzuki, H., Dobson, R. C., Leustek, T., Triassi, A. J., Wheatley, M. S., and Hudson, A. O. (2014) Differential response of orthologous L,L-diaminopimelate aminotransferases (DapL) to enzyme inhibitory antibiotic lead compounds, *Bioorg Med Chem 22*, 523-530.

[5] Laue, T. M. (1992) Computer-aided interpretation of analytical sedimentation data for proteins, *Analytical ultracentrifugation in biochemistry and polymer science.*, 90-125.

[6] Schuck, P., Perugini, M. A., Gonzales, N. R., Howlett, G. J., and Schubert, D. (2002) Size-distribution analysis of proteins by analytical ultracentrifugation: strategies and application to model systems, *Biophys J 82*, 1096-1111.

[7] Ortega, A., Amorós, D., and García de la Torre, J. (2011) Prediction of Hydrodynamic and Other Solution Properties of Rigid Proteins from Atomic- and Residue-Level Models, *Biophysical Journal 101*, 892-898.

[8] Petoukhov, M. V., Franke, D., Shkumatov, A. V., Tria, G., Kikhney, A. G., Gajda, M., Gorba, C., Mertens, H. D., Konarev, P. V., and Svergun, D. I. (2012) New developments in the ATSAS program package for small-angle scattering data analysis, *J Appl Crystallogr 45*, 342-350.

[9] Konarev, P. V., Volkov, V. V., Sokolova, A. V., Koch, M. H. J., and Svergun, D. I. (2003) PRIMUS: a Windows PC-based system for small-angle scattering data analysis, *Journal of Applied Crystallography 36*, 1277-1282.

[10] Svergun, D. (1992) Determination of the regularization parameter in indirect-transform methods using perceptual criteria, *Journal of Applied Crystallography 25*, 495-503.

[11] Panjkovich, A., and Svergun, D. I. (2016) Deciphering conformational transitions of proteins by small angle X-ray scattering and normal mode analysis, *Phys Chem Chem Phys 18*, 5707-5719.

[12] Battye, T. G., Kontogiannis, L., Johnson, O., Powell, H. R., and Leslie, A. G. (2011) iMOSFLM: a new graphical interface for diffraction-image processing with MOSFLM, *Acta Crystallogr D Biol Crystallogr 67*, 271-281.

[13] Winn, M. D., Ballard, C. C., Cowtan, K. D., Dodson, E. J., Emsley, P., Evans, P. R., Keegan, R. M., Krissinel, E. B., Leslie, A. G., McCoy, A., McNicholas, S. J., Murshudov, G. N., Pannu, N. S., Potterton, E. A., Powell, H. R., Read, R. J., Vagin, A., and Wilson, K. S. (2011) Overview of the CCP4 suite and current developments, *Acta Crystallogr D Biol Crystallogr 67*, 235-242.

[14] Vagin, A., and Teplyakov, A. (2010) Molecular replacement with MOLREP, *Acta Crystallogr D Biol Crystallogr 66*, 22-25.

[15] Murshudov, G. N., Vagin, A. A., and Dodson, E. J. (1997) Refinement of macromolecular structures by the maximum-likelihood method, *Acta Crystallogr D Biol Crystallogr 53*, 240-255.

[16] Adams, P. D., Afonine, P. V., Bunkoczi, G., Chen, V. B., Davis, I. W., Echols, N., Headd, J. J., Hung, L. W., Kapral, G. J., Grosse-Kunstleve, R. W., McCoy, A. J., Moriarty, N. W., Oeffner, R., Read, R. J., Richardson, D. C., Richardson, J. S., Terwilliger, T. C., and Zwart, P. H. (2010) PHENIX: a comprehensive Python-based system for macromolecular structure solution, *Acta Crystallogr D Biol Crystallogr 66*, 213-221.

[17] Emsley, P., Lohkamp, B., Scott, W. G., and Cowtan, K. (2010) Features and development of Coot, *Acta Crystallogr D Biol Crystallogr 66*, 486-501.